NBSIR 88-3767

Products of Wood Smolder and Their Relation to Wood-Burning Stoves

T. Ohlemiller
W. Shaub

U.S. DEPARTMENT OF COMMERCE
National Bureau of Standards
National Engineering Laboratory
Center for Fire Research
Gaithersburg, MD 20899

May 1988

Sponsored by:

U.S. Department of Energy
Washington, DC 20585

NBSIR 88-3767

PRODUCTS OF WOOD SMOLDER AND THEIR RELATION TO WOOD-BURNING STOVES

T. Ohlemiller
W. Shaub

U.S. DEPARTMENT OF COMMERCE
National Bureau of Standards
National Engineering Laboratory
Center for Fire Research
Gaithersburg, MD 20899

May 1988

Sponsored by:
U.S. Department of Energy
Washington, DC 20585

U.S. DEPARTMENT OF COMMERCE, C. William Verity, *Secretary*
NATIONAL BUREAU OF STANDARDS, Ernest Ambler, *Director*

TABLE OF CONTENTS

LIST OF TABLES

LIST OF FIGURES

PRODUCTS OF WOOD SMOLDER AND THEIR RELATION TO WOOD-BURNING STOVES

T. J. Ohlemiller and W. Shaub

Abstract

The smoldering combustion of solid wood is a process pertinent to both fire safety and to the generation of air pollutants in wood burning stoves; fundamental aspects of this process are examined here in order to provide insights into both of these problem areas. The wood configuration employed here was designed to permit self-sustained smolder with visual access. The sample was in the form of a U-shaped channel 74 cm long with 6.4 cm thick walls. This sample was contained in a steel chamber which confined incoming air to flow along the interior of the channel. Smoldering was initiated on the interior surface of the upstream end of this channel and it propagated in the same direction as the airflow (forward smolder). Tests were conducted with both red oak and white pine and both woods behaved quite similarly. In separate tests the air flow velocity (referred to the initial cross section of the channel) was varied from about 9 to 22 cm/sec. At the low end of this range, the smoldering process was prone to extinction; at the high end it was increasingly likely to transition into flaming combustion. The smolder velocity, peak temperature, rate of heat and product evolution all increased over this flow range in an essentially linear manner. Analysis of the temperature profiles in the wood pointed to a dominance of radiative transfer in the smolder propagation process at low air flow rates and roughly equal roles for radiation and convection at higher flow rates. The principal species in the tar evolved from smoldering wood resemble, in large degree, those from previous forced wood gasification experiments and those obtained from a wood stove operated in a smoldering mode. This reinforces the previous conclusion that air pollutants arise directly from wood smolder and change little in passing through the firebox of a stove. Estimates of the kinetic rates of destruction of several of these species by pyrolysis and by oxidation further reinforce this idea. These same estimates imply that pollutant

species generated in a smoldering mode cannot be destroyed without either a drastic re-design of the wood stove or the use of some form of afterburner.

1. INTRODUCTION

This report is a sequel to a previous publication entitled "Products of Wood Gasification" [1]. Both that and the present report address the gasification of wood in an attempt to shed light both on the fundamentals of wood combustion and on the origins of the pollutant species that are emitted from wood-burning stoves. In the previous study, the non-flaming gasification of wood was examined in a highly idealized configuration -- the samples were 4 cm. cubes irradiated on one face. The effects of the large number of parameters in that problem were examined one by one. Thus the effects of heat flux and duration, ambient oxygen level, wood grain orientation, wood type and moisture content, and sample thickness were all examined. For realistic ranges of each of these variables taken individually, the changes in the proportions of the various products (both gaseous and liquid) were rather limited, being generally in the range of a factor of two or three.

The condensible products formed in that study were "fingerprinted" by means of capillary gas chromatography. These fingerprints showed substantial similarity to those from condensible products captured in the exhaust stack of a wood stove operated in a smoldering mode (inlet air cut down to the point that flames were absent and the only combustion was due to surface oxidation of the wood char). This mode is frequently used to produce extended burns from a single load of wood and it produces copious air pollution. The fingerprint comparison just noted suggests that the origin of most of these air pollutants is at and below the wood surface during its gasification and that little further chemical change occurs in the stove before these species exit the stack (for this smoldering mode of burning). That, in turn, implies that the pollution problem is inherent in the use of wood in the smolder mode; only some post-smolder intervention (e.g., an after-burner) would help to eliminate the pollutants.

The previous results are all based on the use of forced gasification (due to the externally applied heat flux) and an essentially one-dimensional heat flow geometry. This is a potentially deceptive over-simplification of the actual behavior of wood in a fire or in a wood stove. In these real-world cases, the smolder zone is multi-dimensional and it spreads outward from a limited portion of the fuel where it began. Furthermore, it does so in a self-sustaining manner that does not require some external heat input. Since this produces a different temperature distribution and a different blend of pyrolysis and oxidation regions, one might well expect that the product distribution could differ from that seen in the one-dimensional, forced gasification cases. Examining this issue is one motivation for the present work.

A second motivation for studying the self-sustained smolder case is that it contains within it a relation between the rate of air supply and the rate of wood gasification which is of use in estimating the rate of pollutant or toxicant emission from this mode of combustion. This relation will be applied here in estimating the feasibility of destroying the pollutants from wood stoves by gas phase reactions.

In estimating the feasibility of destroying pollutant species by gas phase reactions, one needs estimates of the relevant rate processes. These estimates have been obtained here by the methods of chemical kinetics.

A third motivation for studying the self-sustained smolder of solid wood is that, despite its relevance to both wood stoves and to fire safety, it has not been examined before in any quantitative detail. For the purposes of fire safety hazard assessment, one needs, at a minimum, the rate of heat release from the smoldering wood and the rate of toxicant generation (principally CO). However, one would also like to have some insights into the factors which control the rate of smolder spread over the wood. All of these points will be addressed in varying degree.

2. EXPERIMENTAL APPARATUS AND PROCEDURE

2.1 Sample Configuration

There is no standard configuration for wood being burned in a wood stove. Any geometry that attempts to closely mimic a pile of split logs is clearly going to introduce complexities that only serve to make interpretation more difficult. The objective here is a simple geometry with which it is easy to interpret the behavior of a spreading, self-sustaining smolder reaction wave.

A single flat slab of wood which is thermally thick (actual thickness greater than the depth of a thermal wave originating at the slab surface) will not sustain smoldering combustion unless an external heat flux supplements the heat from wood char oxidation. Preliminary experiments established that this external heat flux needs to be greater than about 1 W/cm^2. Although a flat slab geometry would certainly be desirable for its simplicity, it is not practical for the present case. The added heat flux would have to irradiate only the active reaction zone; this would require that it move with the spreading reaction zone at a rate whose value would be hard to pin down.

Instead of trying to impose a moving heat source, it is better to choose a geometry which produces its own; this assures truly self-sustaining smolder spread. Two flat slabs of wood with an air gap between them have been used in the past [2]. Smoldering on each interior slab face provides the sustaining flux for the face opposite. However, unless the air gap is wide, this configuration provides limited visual access to the smolder zone.

The configuration that was used here is shown in Figure 1. It is a flat bottom U-shaped channel; smoldering spreads along all three interior surfaces of the U. This approximates a closed channel which is sometimes used as an idealization of the flow passages through a burning bed of fuel particles [3,4]; the geometry used here then can be viewed as an idealization of that occurring in a wood stove with a fuel load on a grate and an air flow coming up through the grate into the bottom of the fuel bed. An observer looking into the open side of the U has a good view of the smolder behavior on the

bottom of the U and an oblique view of the other two surfaces. The original intent was to exploit this direct view of the bottom of the U by using an imaging infrared radiometer to track the surface temperature distribution there. This proved to be impractical due to obscuring window deposits. However, the bottom of the U remained a natural focus for assessing the behavior of the smolder spread process.

Note that the sides of the U channel each consist of two pieces of wood 3.2 cm thick. Full thickness (6.4 cm) wood was not available in either of the two wood types used (white pine and red oak). The two pieces were glued together (Titebond Wood Glue, Franklin Chemical Industries)[1] and further held by a small number of wood screws, especially near the end to be ignited. The three composite side pieces were similarly glued and screwed together to form the U channel shown in Figure 1. There was some tendency for the U channel to attempt to warp during a test in such a way as to partly close the open side of the U; this was prevented by placing a series of four rigid steel spacers in this open side at intervals along the channel.

The height-to-width ratio of the U channel is such that, if the long sidewalls were uniformly hot, the radiation from them would produce an essentially uniform flux over the lateral expanse of the bottom of the U. Preliminary tests indicated that, at least for the igniter size used here, the noted ratio could not be decreased much below the value used here without precluding smolder propagation but this subject deserves further study in the future.

2.2 Wood Combustion Chamber

The wood sample was enclosed in a combustion chamber in order to provide for control of the flow of air and combustion products; Figure 2 shows a schematic of this chamber. The actual orientation of the sample was the same as that

---

[1] In order to adequately describe equipment , it is occasionally necessary to identify commercial products by manufacturer's name. In no instance does such identification imply endorsement by the National Bureau of Standards nor does it imply that the particular product or equipment is necessarily the best available for that purpose.

shown in Figure 1. The walls are 1.27 cm steel and they form an enclosure only slightly larger than the wood sample itself. Any gaps (above and below as well as toward the open end of the U) were filled with layers of ceramic fiber insulation wrapped in aluminum foil; thus the outer surfaces of the long sides of the U were backed by 1.3 cm of insulation while the bottom of the U had no insulation. Flow was thereby constrained to pass only along the interior of the U channel.

A controlled flow of air at ambient temperature entered the left end of the chamber in Figure 2 through a 1.26 cm ID pipe fitting; no attempt was made to condition the air stream with regard to turbulence. However, instead of simply entering as an axial jet, the air was deflected by a plate in front of the pipe opening into four streams tangential to the end plate of the chamber. This caused mild turbulence in a stream that would otherwise be judged to be laminar from the Reynolds number in the U channel.

The chamber has a series of five Vycor windows set in water-cooled frames which provide visual access to the interior of the U channel. As noted above, these had a definite tendency to become coated with condensate during the course of a test but this generally did not preclude visually following the glowing combustion zone.

For the tests reported here, the igniter was always placed at the upstream end of the U channel, producing smolder spread in the same direction as the air flow. This is called forward smolder. (Other cases will be examined in the future.) The igniter consisted of a set of three separately controlled electrical heaters, each spaced about 6 mm from an interior surface of the U channel. They were each operated from a separate constant temperature controller. They heated a length of the channel of about 12 cm.

2.3 Associated Equipment

Exhaust gases exited from the right end of the chamber as seen in Figure 2. The collector cone at that end and the subsequent transfer lines were heated as shown schematically in Figure 3; the lines could not be kept isothermal but

were generally in the range from 150 to 200°C. This was not sufficient to preclude some deposition of heavy tars which subsequently formed a thin char coating on the interior of all the stainless steel transfer lines. This appeared to represent a very minor loss mechanism for products on a weight basis though it could represent species of interest for air pollution studies.

The somewhat complex arrangement of plumbing downstream of the wood chamber reflects two factors: 1) it was not feasible to push flow through the chamber while the igniter was in place; instead it was pulled through by the pump indicated in Figure 3; 2) it was not desirable to send the exhaust flow through the gas analyzers continuously, thus they were sampled intermittently. In light of these there were two flow paths used most of the time. During ignition all exhaust flow went through the pump (Air-Vac TD 260 air driven venturi pump). The inlet closure plate was removed from the left end of the chamber and room air was drawn onto the U channel. There was no super-atmospheric pressure in the chamber to force gases into the analyzers so no gas analyses could be done during the ignition interval. After ignition, the left closure plate was installed and the indicated components fed laboratory air to the chamber. The internal pressure in the chamber was thus slightly elevated (1.02 to 1.06 atm.). The main flow path was then through the water cooled heat exchanger indicated schematically in the lower right area of Figure 3. This device was utilized merely to lessen the load of condensate going into the laboratory exhaust system. At intervals the full flow from the chamber was switched from the heat exchanger path to the path with a large condenser coil (surrounded by a dry ice/ethanol slush at -72°C) followed by a filter and a dry gas test meter (Singer DTM-115 or DTM-325) for volumetric flow measurement. This permitted sampling of the condensate for later gas chromatographic fingerprinting and also for assessing its mass flow rate. The dry gas test meter results, together with separate determination of the average molecular weight of the gas, permitted calculation of the total mass flow rate from the wood chamber. At other times, part of the flow was diverted, again through a condensate trap and a filter, to a set of gas analyzers. These included a Beckman polarographic oxygen analyzer, an Infrared Industries Model 702 CO/CO_2 analyzer and a Beckman Model 402 total hydrocarbon analyzer. The oxygen analyzer was calibrated with room air before

each measurement; the other two analyzers were calibrated before each smolder test.

In addition to product analyses, information was obtained on the internal temperature profiles in the wood as the smolder reaction zone moved past the region of measurement. Nine thermocouples (chromel/alumel in 1.02 mm dia. stainless steel sheaths) were embedded in the bottom of the U-shaped wood channel. Their junctions were on the centerline of this piece and they penetrated the wood from the side which is on top in Figure 1. They were arrayed in three groups of three thermocouples as diagrammed in Figure 4. Since the thermocouples had to penetrate about 10 cm of wood, from the chamber wall inward, special precautions were taken to assure that the junctions ended up spaced the same as the entry points as shown in Figure 4. A 7.5 cm long drill guide was used to orient a 3 mm dia. pilot drill that stopped about 2.5 cm short of the intended depth of the thermocouple junction. The remaining depth was then drilled just slightly larger in diameter than the thermocouple sheath to assure its good contact with the wood. The thermocouple outputs were recorded at ten minute intervals by a datalogger.

The design of the experiment include following the weight of the sample inside of the chamber by means of weighing both together. The chamber is an order of magnitude heavier than the sample but a highly sensitive balance was obtained to overcome this problem. Unfortunately, the total weight somewhat exceeded the balance capacity and it was necessary to displace some of the weight onto a pivot point (through which the inlet and exhaust lines for the chamber passed). The arrangement proved to be unworkable since thermal expansion of the exhaust line caused a varying force on the balance comparable to the sample weight loss. There was no opportunity to correct this arrangement during the course of the present experiments and so the balance provided no useful data; this will be corrected in future tests.

2.4 Test Procedure

The U channel was assembled typically a few days before a test from wood that had spent one or more months in conditioned storage (50 ± 5% R. H. at

23 ± 2°C). The wood itself was originally kiln-dried; both the white pine and red oak used were knot free.

After the sample was inserted in the chamber, the transfer lines were brought up to temperature. Since the collector cone at the end of the chamber was also heated, this caused some pre-heating of the right end of the sample. The smolder reaction zone never got more than about halfway along the U channel during a test so this remote preheating should have had little effect.

When the lines were adequately heated, the igniter was brought up to temperature over a period of a few minutes. The igniter temperature was typically 450°C for white pine and 500°C for red oak. Higher temperatures might well have accelerated the ignition process but they run the risk of flaming ignition as well. Ignition was, in fact, quite slow requiring about 1½ hours for white pine and about three hours for red oak. The air flow during this time was in the same range for all of the tests, 90 (+5, -10) g/min. Because the balance system did not work, the weight loss from the sample at the end of the ignition period could not be determined directly; it was estimated from the fact that the volume of wood consumed at this point was about the same in all cases.

After the igniter was removed, the inlet end of the chamber was sealed and the incoming air flow was set at the desired value. The intent was always to hold it constant from this point onward but there were occasional complications. In two cases, gradual accumulation of charred residue in the smallest diameter region of the exhaust gas transfer line caused a slow decay in the flow rate. In a few other cases near the borderline for transition from smoldering to flaming, the flow was deliberately cut back when it appeared that flaming was imminent due to bright, localized glowing of the char. In all but one case the flow was restored to its original level within a few minutes.

The rate of spread of the smolder reaction zone after ignition was quite slow, even in high air flow cases. Thus it was possible to follow its progress for up to seven additional hours and still have the reaction front move less than 2/3 of the way along the U channel. In general this post-ignition time was

made as long as feasible in order to lessen the relative role of the ignition period in the overall sample weight loss. Visual observations were recorded as to the position of the leading edge of the smolder front and, where possible, the length of the glowing char oxidation zone.

Up to three condensate samples were taken during the post-ignition smolder period. Typically, a substantially greater number of permanent gas analyses were made in this same time period. The maximum quantity of condensate that could be captured in the cold trap was sometimes severely limited by a tendency for ice to block flow through the trap; this will be fixed in future tests.

Smoldering was terminated by replacing the air flow with pure nitrogen. The sample was removed from the chamber the next day and weighed to determine total weight loss (ignition plus post-ignition).

Time limitations precluded an extensive series of tests; ten fully instrumented runs were made after nine preliminary runs that explored the necessary sample configuration, minimum air flow and ignition conditions.

2.5 Condensate Analyses

Ethanol was used to flush the condensate from the glass cold trap. This mixture was then analyzed in two ways. The first involved capillary gas chromatography to obtain fingerprints that could be compared with those from the previous test configurations [1]. For this reason the analyses were done in, as nearly as possible, the exact same manner. The same type of column was used (J & W DB-1701, although it was necessary to replace it with a new unit) together with the same carrier flow and temperature programming. The fingerprints thus obtained consisted of the chart produced by a Hewlett Packard 3390A Chromatographic Integrator. This chart is a record, about six feet in length, of the pattern of peak elution from the column over a period of two hours. The peak pattern contains features due to relative retention times and characteristic peak shapes that make it possible to compare fingerprints with those obtained previously without a need to repeat any of

the mass spectral analyses that were reported before [1]. It is worth repeating an observation made in the previous work. The majority of the condensible organic species in the cold trap are not volatile enough to come through the chromatograph column, evidently because they have polymerized. It was previously estimated that the about 80% by mass does not elute from the column.

The second chromatographic analysis on the condensate from the cold trap was intended to quantify the amount of condensible organic species (tar) in the trap. This was done indirectly by analyzing for the two well-defined components in the mixture, ethanol and water on a modified Porapak QS column. In spite of some improvements in technique such as the use of a surfactant to homogenize the tar/ethanol/water mixture, the results of these analyses had very poor reproducibility. This was due in large part to the small fraction of tar in the mixture which made its determination by difference less accurate.

3. WOOD SMOLDER: RESULTS AND DISCUSSION

3.1 Overall Behavior of Wood Smolder

The igniter and, subsequently, the smolder process the igniter induced first pyrolyzed the wood to a char then oxidized that char so that only a fluffy, gray-white ash remained. Typically the igniter was removed when this ash was beginning to form on a front about 2½ to 3 cm downstream from the end of the igniter; the wood around the igniter was gasified to an estimated average depth of about 2½ cm at this point. If the igniter was removed too soon, the smolder process extinguished within a few minutes. This happened occasionally and the igniter was simply put back into place and left for another half hour or so.

After the igniter was removed and the air flow was set at the desired value, the progress of the smolder front in the downstream direction was noted at intervals. The same sequence noted above was occurring, now stretched longitudinally along the length of the U channel -- heat from the char

oxidation zone upstream was fed downstream where it dried, pyrolyzed and charred the wood, then induced the oxidation of the char leaving only an ash residue. The progress of this complex reaction zone was basically steady, i. e., the smolder velocity on the inner surface of the U channel was constant on average. The leading edge of the char oxidation zone was not flat or even, typically, because of the random disturbances introduced by shrinkage cracks in the wood. However, plots of the position of the leading edge of the ash or glowing zone as a function of time over the course of a several hour burn gave rather good straight lines for most tests. This constant average rate of movement has been seen in other two-dimensional, forward smolder processes [5,6] but it was less expected here because the thermal wave in the solid phase is very long (longer than the sample) and the total distance burned over the entire test duration is short compared to this thermal length. Evidently the wood is, in effect, evenly pre-heated over the length burned here. It will be seen later that the progress of the char oxidation front is not limited by the disappearance of oxygen and, instead, appears to be limited by the rate of heat transfer to the unburned wood.

The char oxidation zone extended upstream for a substantial distance from its leading edge; it was of the order of 20 cm long and probably varied with the air flow rate but good data on this are not available. It was over the length of this char oxidation zone that the channel cross section opened up considerably. This zone was terminated on the upstream end by quenching, particularly at the bottom of the U with its lack of insulation behind the wood. Typically, more than a centimeter of charred and uncharred wood were left when the reaction ceased on the upstream end. Because of the varying channel cross section in the reaction zone, all flow velocities given below are referred to the original U channel dimensions (with the gas at room temperature).

As noted above, the wood cracked randomly as it charred, though the cracks were oriented predominantly either along the longitudinal axis of the channel or transverse to it, presumably due to the wood grain orientation. The cracks did not seem to play a major role in the propagation process except, perhaps at very low air flow velocities. There the char reaction seemed to move

preferentially in the cracks, possibly because they afforded a lesser radiative heat loss rate. Shrinkage of the wood also caused separation of the two pieces which made up each side of the U channel. Again this did not seem to play a significant role for propagation under most conditions. It provided more crevices for the smolder to hide in at low air velocities. It may have played some role also in the development of flaming at high air flow velocities. The transition to flaming seemed to be associated with the development, over a period of several minutes, of regions of the char (several centimeters in longitudinal extent) which became hotter (as determined by their brighter glow) than surrounding regions of the char. This could have been facilitated by oxygen penetration into the gap between the two layers of wood causing heating from both sides for the innermost layer; there are no data to confirm this speculation more directly.

3.2 EFFECT OF VARYING AIR FLOW RATE ON OVERALL BEHAVIOR

Smolder propagation rate. The air inflow rate was varied from the extinction limit to the flaming limit, a range which proved to be rather narrow for the present wood chamber configuration. Figure 5 shows the variation of the surface smolder propagation rate with air flow rate between these limits. As expected, the smolder spread rate increases with increased air flow into the upstream end of the U channel. This is consistent with the behavior of forward smolder in other configurations [4,5]. The increased flow of air accelerates the rate of transfer of oxygen to the wood char surface on the interior of the U channel. This, in turn, increases the rate of char oxidation at and below the surface. The attendant increase in the rate of heat evolution in the surface region raises its temperature thereby increasing the rate of heat transfer to unburned portions of the wood downstream and this causes the smolder front to move downstream more rapidly. Figure 6 shows that the char surface temperature does indeed increase substantially with increased air flow rate. These temperatures were the peak values seen by the initially submerged thermocouples (the shallowest in Figure 4); the thermocouples penetrated the char surface when it receded due to char consumption.

The smolder spread rates for white pine and red oak are essentially equal for a given air flow rate. The least squares lines fitted to each set of data points differ, as seen in Figure 5, but, in view of the data scatter, these lines cannot be said to be significantly different. The data in Figure 7 derive from a different measurement, that of weight loss averaged over the post-ignition period[2]. The average weight loss rate for red oak is 1.6 to 1.8 times greater than for white pine. This is consistent with essentially equal smolder propagation rates if one factors in the fact that red oak is about 1.6 times more dense than white pine. Given this density difference, however, equality of smolder spread rates is unexpected. In one-dimensional forward smolder through a permeable bed of wood fibers, Ohlemiller and Lucca [7] found the propagation rate of the char oxidation zone to be limited by oxygen consumption and char oxidation stoichiometry. If the same mechanism applied here, it would imply that the spread rate over oak would be about 40% slower than that of white pine. On the other hand, Ohlemiller [6] found that the rate of heat transfer to the unburned fuel can play a direct role in the propagation rate for two-dimensional smolder of permeable fuel layers. With this in mind, one notes that the thermal conductivity of wood is proportional to density [8] and then expects that oak might propagate smolder faster than white pine. It will be seen below that heat transfer plays a central role here but that conduction through the wood does not; thus the equal propagation rates can be rationalized.

Flaming limit. Transition to flaming combustion was encountered at about the same air flow velocity (20 to 25 cm/sec) for both types of wood. The transition process was unpredictable as to its time of occurrence. It appears that it becomes an increasingly likely event as one approaches the upper end of the air flow range in Figure 5. Thus it will occur earlier in a test when the flow rate is 25 cm/sec than when it is 20 cm/sec.

---

[2]The sample weight was only measured before and after a test. The weight loss during ignition was estimated from the observation that the volume of wood gasified at the end of the ignition period was approximately the same from test to test. The weight of this wood volume (approx. 1000 cm^3) was subtracted from the total weight loss to estimate post-ignition weight loss.

As noted previously, the transition process (i.e., the initiation of flaming in the gas phase) was typically associated with localized regions of greater than average char surface temperature. Transition to flaming has three requirements: (1) a local gaseous mixture of fuel and oxygen that is above the flammability limit at the local temperature; (2) a heat source within this gas mixture sufficiently hot to ignite the gases; (3) if the flame is to be sustained beyond a momentary flash, a continuing source of fuel gases, usually assured by heat feedback from the flame to the solid fuel surface. If the local temperature and the gas mixture volume are sufficient, self heating can replace the extra heat source called for in (2). In the present complex configuration, (3) could possibly be met by a combination of gases generated by smoldering and by flaming.

It seems quite probable that the cracks in the char provided local spots which favored the build-up of greater than average concentrations of flammable gases since they would be subject to lesser mass transfer rates than regions of the char surface forming the interior walls of the U channel. In this regard, it is pertinent to address what is known about the concentration of flammable gases in the U channel. Gas analyses were done only on the average composition leaving the channel; these are discussed in greater detail below. For now it is relevant to note that the average CO concentration in the exhaust gas was in the range from 2 to 3%; the total hydrocarbon concentration was in the range from ½ to 1%. At room temperature the lower flammability limit of CO is 12.5% [8]. The total hydrocarbons were not analyzed in the current work but in the previous tests with the same woods they were found to consist largely of methane, ethane and ethylene [1]. The lower flammability limits for these species at room temperature range from just under 3% to about 6% [8]. The lower flammability limit decreases very slowly with increasing temperature; e.g., that of ethane drops from about 3% at room temperature to just under 2% at 550°C [8]. As will be seen below, there is some oxygen depletion along the length of the U channel; again this has only a small effect on the lower flammability limit [8]. On the basis of CO and total hydrocarbons, then, the average gas composition is not flammable for any of the test conditions.

There is another potentially significant source of fuel vapors, the condensible material denoted as tar previously. This constituted about 5% of the exhaust gas mass. If all of this material was in the gas phase in the same locale as the other two fuels, it would almost certainly make a flammable gas mixture. The most likely place for this to occur, however, is in the pyrolysis zone downstream of the char oxidation zone; here the temperatures are too low to ignite the mixture.

In any event, it is clear that the hydrocarbons alone do not need a great deal of concentration enhancement above the exhaust level average to be within their lower flammability limit. They are undoubtedly significantly more concentrated in the boundary layer near the char surface and in cracks in the char. Thus, in the absence of direct local measurements, one can still make the reasonable inference that flammable mixtures exist at many points along the hot char surface. If so, the factor limiting the appearance of flaming is the temperature; the char must get hot enough in a region adjacent to one of these flammable mixtures to ignite it. Momentary flash ignitions were not observed so evidently requirement (3) above is readily met, though it is not clear just how. Direct sampling of the gases within the U channel is needed to test the ideas expressed here.

If temperature is the controlling variable in transition to flaming with wood in this configuration, one might expect some apparatus dependence for the air velocity at which the transition occurs. The temperature achieved for a given rate of heat generation (corresponding to a given rate of air inflow) is somewhat dependent on the rate of heat loss which, in turn, depends on apparatus design. It is interesting to note that Alexopoulos and Drysdale obtained comparable air flow velocities for transition to flaming with forward smolder upward in an insulated chimney lined with wood-based fiber board [9]. Evidently the critical air velocity value does not vary rapidly with heat loss conditions.

Extinction limit. The lower limit to smolder propagation, extinction, was only actually seen with white pine. The smoldering in the lowest air flow case for red oak in Figure 5 was clearly quite weak, however. Interestingly,

the extinction with white pine occurred after the sample had smoldered for about six hours beyond the end of the ignition interval. Form the propagation rate in Figure 5(a), it is apparent that, even in this time, the smolder front moved only a few centimeters downstream. The preponderant smolder process then was inward penetration into the wood and it was probably stopped by quenching when the remaining thickness of wood could no longer provide sufficient insulation. This suggests that this lower limit could probably be extended somewhat by using thicker wood walls and providing more external insulation for them.

Effective fuel to air ratio. The ratio between the rate of wood gasification and the rate of air inflow is a parameter one needs in order to estimate the rate of evolution of pollutant species from wood smolder. This parameter is configuration dependent since it affected both by the degree of contact between the wood and the air and also by their relative directions of movement. This last refers to the issue of whether the air flows in the same direction as the smolder front moves (as it does here), the opposite direction, or some combination of the two plus transverse flow as well; these concepts are essentially the same as those embodied in the idea of updraft, downdraft or crossdraft burning modes in a wood stove [10] . For the two simpler cases (flow strictly with or against the direction of smolder propagation) as they occur in a bed of porous fuel, it has been shown that this fuel to air ratio differs considerably [7]. Configuration dependence has not yet been investigated in the present context but the result just noted implies that caution is necessary in using the present result for other configurations. Where data are available for wood stoves, this ratio has been found to vary by at least a factor of four [11].

Figure 8 shows the results obtained here for the ratio of post-ignition weight loss rate to average air inflow rate. Given the scatter in the oak data, it cannot be said that this ratio changes significantly with air flow velocity. The ratio once again shows more red oak being gasified with the ratio for the two woods being approximately in the ratio of their densities. The values of the fuel to air ratio obtained here fall at the high end of the range seen for wood stoves [11]. In wood stoves operated with a very limited air supply rate

(where one might expect a predominance of smoldering) the ratio tended to be lower than the range seen here; there it varied from 0.04 to 0.10 [11]. The stove tests used 5 by 10 cm and 10 by 10 cm oak brands stacked in the fire box; the air flow was apparently a crossdraft.

As will be seen below, oxygen consumption was not complete in the configuration used here. When the fuel consumption data are recomputed on the basis of the oxygen actually consumed, one obtains the results in Figure 9. Again more red oak was gasified relative to white pine in approximately the ratio of the density of the two woods. These comparisons between the two woods in all cases suggest that the smolder zone moved down the U channel gasifying the two woods at an equal volumetric rate (for a given air inflow rate) independent of wood type.

The data in Figure 9 reflect the incompleteness of the wood oxidation in the present smoldering combustion mode. Stoichiometric oxidation of the two woods requires that the ratio in Figure 9 be in the range 0.5 to 0.7; these stoichiometric values are based on pitch pine and white oak, the closest woods for which elemental compositions were available [12]. It is this high degree of incompleteness which makes this combustion mode so polluting. This is reflected also in the composition of the evolved gases which is examined below.

3.3 Composition of the Evolved Products

Time-dependent composition of the gases. Figures 10 through 19 show the variation of the major products with time from post-ignition to the end of each test.

The first point to note is that, in all of the tests, there was a considerable amount of oxygen passing along the entire length of the sample without being consumed. The reason for this is basically the same as it is in many wood stoves; the contact between the incoming air stream and the hot char surface is not sufficient. For the present configuration one can readily calculate that an oxygen molecule entering the reaction zone on the centerline of the U

channel will convect more than the full length of this zone before it can diffuse laterally to the char wall. The original intent was to run the air flow sufficiently slowly that there would be time for this diffusion but this called for air flow rates below the extinction level in this apparatus.

A more subtle point concerning the remaining oxygen has to do with the failure of the reaction zone length to grow sufficiently to consume all of that oxygen. If there is plenty of oxygen in the gas at the leading front of the reaction zone, one might expect the front to move downstream until it consumes all available oxygen and then move onward only at the rate at which completion of fuel consumption on the upstream end of the reaction zone permits; this is what happens in forward smolder through a permeable fuel bed [7].

Channel configurations with flow and reaction zone movement in the same direction have been studied in the context of coal and oil shale gasification [13,14] and in the context of flame propagation in fuel-lined ducts [15]. In the first two contexts, complete consumption of oxygen appears to be typical, at least for the conditions described in these references. For fuel-lined ducts with flaming combustion, cases were seen in which oxygen consumption was small and in which the consumption was total; however, in the case of small oxygen consumption, the fire either died out eventually or accelerated to a case of total oxygen consumption. Roberts and Clough [15] presented a simplified analysis of the energy conservation in the duct which implied that two propagation rates are possible but the lower rate, which leaves residual oxygen, is unstable; the solution achieved depends on the vigor of the ignition process. The assumptions in this model do not fit the present problem well. De Ris [16] suggested that the cases of incomplete oxygen consumption were the result of flow stratification in which a layer of cooler, oxygen-containing gas flowed along the bottom of the duct and escaped reaction. In the absence of flow and oxygen profiles within the U channel, it is not certain if such behavior is pertinent here, but it seems doubtful. No stratification of the smoke flow was noted during the tests. Furthermore, the reaction front on the bottom of the channel did not lag behind other portions. It seems more likely that the rate of heat transfer to the unburned fuel downstream of the char oxidation zone in the present configuration was not

enough to permit a sufficient extension of the reaction zone so that all oxygen could be consumed; this will be examined further below.

Another point to be noted about the time-dependent gas composition data in Figures 10 to 19 is that, in most cases, the composition is very nearly steady. This goes along with the previous observation that the rate of propagation was essentially constant. There are two notable exceptions, the tests in Figure 17 and Figure 19; in both cases the air flow rate was in the region of the flaming limit. The decaying oxygen penetration of the reaction zone suggests that the length of the zone was increasing toward the zero penetration case discussed above; unfortunately, confirming data on the length of the reaction zone as a function of time for these cases are not available. The rate of propagation of the reaction front was not accelerating in either case; it was as steady, on average, as other cases of slower air flow rate. For the reaction zone length to grow longer, however, it is only necessary for the rate of longitudinal movement of the smolder front to increase relative to the rate of lateral penetration of the front into the wood. These two rates, which are the orthogonal components of the smolder velocity vector normal to the isotherms in the solid, may not have reached a steady balance in these two cases. This is a situation which could be illuminated by a two-dimensional smolder propagation model which is not available at present.

Also note that in Figures 17 and 19 there is a an increase in the ratio of CO_2 to CO with increasing time. This is small but evidently real; for example, in Figure 19 the ratio goes from the range 2.4 - 2.6 up to 3.0. This could reflect increased flow time available for gas phase CO oxidation to CO_2 as the smolder zone lengthened. The residence time (flow time) is about one second in these cases and the peak gas phase temperature is about 650°C. Extrapolation of Dryer's [16] kinetics for the homogeneous oxidation of 'wet' CO indicates that some oxidation is possible in these conditions. The characteristic blue flame indicating rapid CO oxidation was not seen here. The heterogeneous reduction of CO_2 to form CO evidently requires somewhat higher temperatures to be appreciable for the times available here [17]. Definitive characterization of the behavior of these gases for this particular

system would require sampling of the composition of the gas phase along the length of the U channel.

Time-averaged compositions. Comparisons with the results of our previous, small scale, forced gasification study of these same two woods is most readily done on the basis of the average composition of the evolved products. The current results are given in Figures 20 and 21 for white pine and red oak, respectively. They are expressed there as fractions of the total product mass in the post-ignition period. The scatter in both of these Figures is such that no real trends with air flow rate can be said to exist. This is in spite of a 200°C range in surface temperatures for the air flow range indicated (Fig. 6). The closest analog to the present series of experiments in the previous small scale forced gasification experiments is that in which the incident heat flux to the surface was varied. Increasing the heat flux there from 2.5 to 6.9 W/cm_2 caused the peak surface temperature to go from about 550°C to about 750°C [18]. For the most part, the variation in the fractional distribution of evolved products over this flux range was not strong but there were significant increases in the fractions of both CO and CO_2. These increases were mainly in the range of 50% but for red oak the increase was markedly stronger for CO. These comparisons between the two types of experiments are rather strained because the forced gasification tests were highly transient in nature and much shorter in time scale (10-15 min.); this biases the products toward those formed early at lower temperatures than the above peak surface values would indicate. This is particularly evident in the case of water which comprised 40 to 60% of the evolved products in the forced gasification experiments and only 20 to 30% of the products here. The wood samples in both test series were equilibrated to the same ambient conditions so that their water contents were quite comparable.

The actual origins of the various major products shown in Figures 20 and 21 is not completely clear. If the char were a pure pyrolytic graphite, its oxidation in the present temperature range would yield only CO_2 [19]. The char formed from cellulose contains amorphous carbon as well as significant amounts of hydrogen and oxygen [20]; this is very likely also true of the char contributed here by the hemi-cellulose and lignin components of the woods.

Oxidation of cellulosic char yields equal amounts of both CO and CO_2 in the absence of inorganic ash; differing ash components alter this ratio appreciably [21]. The previous forced gasification experiments were performed in nitrogen as well as air; those results imply that in the current tests the majority of the CO and CO_2 arises from char oxidation. The remainder comes both from pyrolysis of the wood components (particularly holocellulose) and from secondary degradation of the tar components.

Degradation of wood tar was studied by Boroson [22]. Tar generated by pyrolysis of the components of wood can undergo two classes of reaction as it passes out through the bulk of the sample (through the char layer typically on the sample exterior) and into the surrounding gas phase. The first class comprises homogeneous pyrolytic reactions, probably unimolecular in nature.; the second class comprises heterogeneous reactions between the tar components and the char surface over which they pass as they exit the sample. The homogeneous reactions typically convert a fraction of the tar to gases, the major one being CO. The fraction converted is dependent on temperature and, at a given temperature, is essentially fixed after about one second (particularly at temperatures above 600°C). The homogeneous reactions are very fast and affect only a fixed fraction of the tar independent of times longer than a few milliseconds and independent of temperature, at least in the range from 400 to 600°C. The fraction of tar undergoing this heterogeneous reaction was estimated to be about 1/3. The products were mainly CO, CO_2 and char.

In the context of the present experiments, Boroson's results imply that anywhere from zero to 50% (over the temperature range in Figure 6) of the initial tar generated within the pyrolysis zone of the wood was degraded by homogeneous pyrolysis. One can estimate that it takes O(1-10 sec) for the gases generated within the sample to pass through the char layer; the subsequent time in the gas phase passing along the length of the reaction zone in the U channel is O (1 sec). Thus essentially all of the homogeneous degradation of the initial tar occurs within the sample. The same holds true, of course, for the heterogeneous degradation. The combined degree of

degradation of initial tar thus varies from 1/3 to about 5/6, based on Boroson's results applied to the present context.

There is a discrepancy between the above inferences based on Boroson's results and the results in Figures 20 and 21. Those Figures show a quantity of surviving tar that is both substantial in amount and constant with air flow (and, therefore, temperature). The above arguments imply that the amount of tar should decrease by about a factor of two as from the lowest to the highest air flow rate. Tar determinations were not very accurate (standard deviation about ±50%) so this could mask any such trend. On the other hand, since CO, in particular, is a major product of the tar degradation, one should see a substantial increase in its weight fraction with increasing air flow rate; the CO analyses are believed to be quite accurate. The reason for this discrepancy is not known.

Figures 22 and 23 show the post-ignition average product information in a different manner, i.e., on the basis of mass of product generated per unit mass of wood gasified. This is the form that is most useful for determining the rate of evolution of toxic or pollutant species from smoldering wood in other contexts where the behavior of wood might be expected to be similar. Note that the sum of the products for any given flow condition need not add up to one even though one gram of wood went into generating them; oxygen from the inflowing air is also incorporated in the products. The average summation of the product masses was,in fact, 1.17 grams per gram of wood gasified; the average deviation is rather large, 0.12. This variability reflects a varying mass balance on the system. The principal errors are believed to reside in the determination of the total mass flow out of the chamber as a function of time and in the estimate of the amount of wood gasified during the ignition process. In addition, as noted previously, the tar fraction values used here have a ±50% uncertainty. The water values are the average of those determined from the water transducer in the exhaust line and the water content of the condensate trap; these typically were about 20% apart. Given these uncertainties and the evident scatter in the data, it is again not possible to say that the products vary in any significant way with air inflow rate.

Similarly, one cannot assert that the products from the two different types of wood are significantly different.

The weight ratio of CO_2 to CO in the previous, forced gasification experiments was in the range from 1.5 - 2.5 to 1. Here it is about 3 to 1. In stove burns done in the first year of this program, the ratio was substantially higher, from 6-9 to 1 [23]; this approaches the value of 10 to 1 seen for flaming combustion in a free-standing fireplace [24] so one cannot rule out the role of flaming combustion in those early stove burns. It seems probable that CO oxidation to CO_2 in the gas phase is the reason that the numbers here and in stove burns exceed those seen in the forced gasification experiments. This comparison also implies that such oxidation is considerably less in the present configuration than it is in a wood stove operated in a slow burning mode [23].

3.4 Condensate Fingerprints

This subject was pursued much more extensively in our previous work [1] where an effort was made to identify many of the species eluted through a capillary gas chromatographic column. Time constraints severely limited the follow-up work with the present condensates (tar) seen in the cold trap. The goal here was only to compare the patterns of species quantity and retention time (i.e., the "fingerprint") that one gets as an output from the chromatograph. Even this presents some technical difficulties, especially in the first 10% or so of the fingerprint where solvent pooling effects[3] lead to non-reproducible retention times.

For white pine, visual matching of the fingerprints indicates a strong degree of similarity between those obtained here and those obtained in the forced gasification experiments. It appears that nearly all of the same components are present in the two types of condensates but there are a small number of

---

[3] The solvent carrying the tar onto the chromatographic column condenses to a liquid at the front end of the column. This liquid spreads unevenly and irreproducibly under the influence of the column carrier gas causing a variable initial distribution of the tars on the front end of the column.

exceptions among the larger peaks, most of which are unidentified. One which has been identified is levoglucosan, a primary product of cellulose degradation. In the forced gasification tests, it was nearly always one of the prominent species in the tar; here its presence could not be confirmed.

Changes in the relative proportions of the eluted species with method of generation are harder to judge precisely. Table 1 shows some data along these lines for eight of the major species in the eluted condensate. Since it is not possible to assure that one is injecting exactly the same total mass of tar onto the chromatograph column with each different sample, the area percentage numbers presented there have normalized by the area of one of the most reproducible peaks, that for creosol. The area percentages shown in the Table are calculated after both methanol, the solvent in the previous tests, and ethanol, the solvent in the present tests, have been subtracted out. Area percentages are only an approximate indication of mass concentration in the tar because detector response factors are not included.

Table 1 shows normalized area percentages for the condensate from the base case of forced gasification and for low and high air flow cases of self-sustained smolder (present work). For white pine one sees there variability in the tars from the present tests of as much as a factor of two to three. This may not be significant, since that degree of variability was seen in the previous tests repeated under identical conditions. Acetic acid was problematical probably because it occurs in the first ten percent of the fingerprint, that most affected by solvent pooling disturbances; it was highly variable and thus was omitted. For the other species, between the base case for forced gasification and the present results, one sees variations of up to a factor of five (furaldehyde and phenol). Comparable variations appear to be present in other unidentified peaks. This implies that the chemical history of the tars in the two types of experiments differs significantly. Unfortunately there is not enough information available to indicate the source of these differences. Experiments similar to those of Boroson [22], but with tar analyses, are needed to clarify this point.

The same qualitative statement about visual matching of fingerprints between the previous and present results holds for red oak, although here there may be more species where the proportions are different between the two types of test. This is not so apparent from Table 1 where the basic story about relative proportions appears to be about the same as for white pine. Interestingly, the visual match between fingerprints obtained here and those obtained from a wood burning stove (for mixed oak species) in the previous study [1] is as good as or better than that noted previously between the wood stove and the forced gasification results. This reinforces the tentative conclusion arrived at previously that there is very little gas phase chemistry occurring in a wood stove when it is operating in a smoldering mode (referred to previously as an "overnight" mode of operation). Again this implies that the pollutant species escaping from the stack of a wood stove operated in this manner arise directly from the wood smolder process in the condensed phase and then pass through the firebox and up the stack without much alteration. The gas phase kinetics discussion below tends to reinforce this idea further.

3.5 Rate of Heat Release

The rate at which smoldering combustion releases heat is of interest both in the context of wood burning stoves and in the context of fire safety; in the latter, one needs the heat release rate in order to predict the transport of combustion products in the buoyant plume which rises above an unconfined combustion source [25]. The present experiment did not include any means for directly measuring the heat evolved from the wood smolder process, but this is not always necessary. For flaming fires, it has been shown that one can accurately estimate the rate of heat of release from the rate of oxygen consumption; the two are related by a factor (13.1 kJ of heat per gram of oxygen consumed) which is nearly constant for most organic materials of interest [26]. This technique has not been previously applied to smoldering combustion and, indeed, it is not completely clear how accurately it can be applied. Smoldering is characterized by incomplete combustion; this is apparent in the Figures just discussed. Huggett [26] has shown that the above factor converting oxygen consumption to heat release can apply with reasonable accuracy not only when CO_2 and H_2O are the combustion products but also when

partial oxidation products (alcohols, aldehydes acids) are formed. The accuracy is less when alcohols and aldehydes are products, however; the absolute error depends on the quantities of each but it only approaches 20% when these are the only products. Here there is a very complex and ill-defined mixture of tars being generated, some of which are undoubtedly partially oxidized; one can only assume, on the basis of Hugget's calculations, that they are not a major source of error.

A further factor to consider is the formation of CO; its heat evolution per gram of oxygen consumed is only 6.9 kJ/g. In the present experiment, not all of the CO comes from oxidation; some is generated directly by pyrolysis of the wood or tar. A direct measure of this pyrolytic fraction is not available; in the previous forced gasification experiments it was about one-fourth of the total CO.

The results shown in Figure 24 are average heat release rates over the post-ignition period. It has been assumed there that all CO comes from oxidation and that all oxygen consumed in partial oxidation of tar components yielded the full heat release characteristic of CO_2 formation. As expected, the rate of heat release increases with increased oxygen inflow. What is not expected is that the two types of wood are indistinguishable. Recall that Figure 7 showed the rate of mass loss for red oak to be higher than that for white pine by a factor about equal to their density ratios (1.6). Figures 22 and 23 show the product distributions for the two woods to be about the same. Then red oak should be generating oxidized products at about 1.6 times the rate for white pine and therefore should be generating more heat in about the same ratio. If this is the case, it is hidden by the considerable data scatter in Figure 24.

To estimate the rate of heat release from forward smolder a different mass of solid wood, one could presumably scale directly with area of wood likely to be involved in the manner here. In practice this could be difficult to estimate but one could at least get an order of magnitude estimate. The same scaling would apply, as a zeroth approximation, for the rate of species generation.

3.6 Temperature Profiles; Implications for Heat Transfer

The set of nine thermocouples imbedded in the wood that formed the base of the U channel provided sufficient information that one can infer the approximate thermal profiles in the wood. Figure 25 shows such profiles for red oak at low and high air flow velocities. The isotherm patterns are shown superimposed on top of tracings of the wood as seen in cross-section; the plane shown bisects the base of the U channel. The positions of the isotherms have been determined by linear spatial interpolation between the nine instantaneous temperatures at nine known locations. The resulting pattern was shifted longitudinally so that the 300°C isotherm sits on top of the approximate demarcation "line" between charred and uncharred wood. (This is actually not sharp enough to be termed a true line.) Note the crack between the two pieces of wood which form the base of the U; the crack does not appear to have much effect on the isotherms. One can also see the irregular regression of the surface caused by both by shrinkage of the wood as it charred and by conversion of some of that char to ash (not shown). It is apparent from the top of Figure 25 that the reaction zone, in progressing from left to right past the fixed thermocouple positions, will eventually expose them to the surface of the oxidizing char and then to the free space within the enlarging U channel. Thus the peak value of the char surface temperature can be measured by the imbedded thermocouples. The isotherms have also been extrapolated to the surface to provide an approximate measure of the surface temperature distribution ahead of the maximum value.

A striking aspect of the isotherms is their very acute angle with respect to the interior surface of the U channel. This implies that the heat transfer in the wood is nearly normal to the channel surface; that in turn implies that heat conduction through the wood plays a minor role in driving the reaction zone forward along the U channel.

It is possible to use the above information to do a more quantitative assessment of the relative contributions of the various modes on heat transfer in this smolder propagation process. This could facilitate extending the present results to other situations.

Three modes of heat transfer are considered: conduction through the wood in the longitudinal direction, convection by the gas flow along the interior of the U channel, and radiation along the interior cavity of the channel. Kanury and Blackshear [27], on the basis of measurements on cellulose cylinders, suggested that an additional mode of preheating is condensation of water and pyrolysis vapors moving down the temperature gradient in the porous structure of the condensed phase. Such movement would be essentially longitudinal in the present grain orientation. Our previous data (Figures 22 and 23) show that the quantities of tar and water are comparable; however, water, with its high heat of vaporization, is expected to be the more significant component in this regard. In fact the temperature data obtained in the present tests show only a water plateau. This tends to be most pronounced near the outer surface of the base of the U channel, probably because of the lack of thermal insulation there. It does not appear that neglect of this has an appreciable impact on the calculations that follow. Water condensation could also help to preheat the inner surface of the channel, supplementing the convection and radiation discussed below. However, the water condensation front is well downstream of the region to be considered here; tar condensation is neglected because it does not appear to be significant.

The longitudinal heat conduction flux through the wood is readily estimated from the temperature profiles shown in Figure 25. This will be done in the plane where the peak surface temperature is just reached. One needs to compute, as a function of depth below the inner surface of the channel, the value of the following expression.

$$-k(T)\ \partial T/\partial x$$

Here k(T) is the temperature-dependent thermal conductivity of the wood; the second term is the temperature gradient in the longitudinal direction. The gradient in the plane of interest is estimated from the temperature profiles. Thermal conductivity data are not available above 100°C; the linear temperature dependence below this temperature is extrapolated for the present purpose [27]; thus, for red oak, along the grain, one has:

$$k(T) = 0.0039\ (T/300),\ W/cm°C$$

The results, which are shown in Figure 26, are discussed below.

The convective heat flux from the gas flowing along the channel to the wall (downstream of the peak temperature point) is more difficult to estimate because a direct measure of the gas temperature is not available. It will be assumed that the gas acts as a plug flow which is initially all at the peak temperature of the charred wood surface. Since it is quite unlikely that the gas over the whole channel cross section gets to this temperature, this will yield an over estimate of the convective heat flux. Given this assumption, one can calculate the temperature of the gas as it proceeds downstream from the initial peak temperature plane by solving the following differential energy balance equation:

$$m_G C_G\ dT_G/dx = -hA_W[T_G - T_W(x)]$$

This simply expresses the assertion that the gas temperature decays as it loses heat to the wall by convection. Here m_G is the mass flow rate of the gas, C_G is the heat capacity of the gas, T_G is the gas temperature, h is the convective heat transfer coefficient, A_W is the channel sidewall area per unit length of channel (the open side of the channel, which has about 14% of its side wall area, is assumed adiabatic for lack of better information; there are recirculation zones between the channel and the windows along the open side which make this a reasonable approximation), $T_W(x)$ is the temperature distribution along the channel wall obtained in Figure 25 by extrapolating the in-depth profiles to the surface as shown; these surface temperatures results are well-fitted by a straight line or a parabola. The above equation can then be solved analytically for T_G. The resulting expression is used to calculate the convective heat flux to the wall:

$$h\ [T_G(x) - T_W(x)]$$

This profile along the longitudinal direction is also shown in Figure 26.

Estimation of the radiative flux from the sidewalls of the U channel to the base of the U requires certain assumptions also. The principal assumptions are that the temperature profile of the sidewalls is the same as that determined from Figure 25 for the base of the U and also that, once the peak surface temperature is achieved on the surface, the surface remains at that temperature for all points upstream (up to the other end of the char oxidation zone). Visual observations of the glowing of the channel walls suggest that these assumptions are reasonable but they have not been quantitatively checked. It is also assumed that the walls remain flat throughout the isothermal region whereas they actually curve irregularly outward as the char is gasified by oxidation; this assumption is less of an approximation at the higher air flows.

With the preceding assumptions one can show that the longitudinal distribution of radiant flux along the centerline of the base of the U channel is given by:

$$q_{RAD}(x) = 2\sigma T_{w,max}^{4}(F-F') + \frac{\ell\sigma}{\pi}\int_{0}^{x'_{max}} [T_w(x')]^4 \left\{ \frac{1}{\ell^2+(x-x')^2} - \frac{1}{\ell^2+a^2+(x-x')^2} \right\} dx'$$

Here σ is the Stefan-Boltzmann constant, $T_{W,MAX}$ is the peak wall temperature, F is the radiative view factor from the isothermal portion of the sidewall to a point on the axis of the U channel base, F′ is a correction to the preceding view factor when the point on the axis of the U channel base is beyond the end of the isothermal portion of the sidewall, ℓ is the half-width of the U channel, $T_W(x')$ is the linear or parabolic fit to the surface temperature in the non-isothermal region, x'_{MAX} is the maximum downstream position to which the integration of the flux from the non-isothermal sidewall region is taken, x is the longitudinal coordinate, x′ is a dummy longitudinal coordinate of integration. The view factors F and F′, which have the same functional form, are obtained from a standard reference [28]:

$$F = (1/2\pi)[\ \arctan(b/\ell) - (\ell/(a^2+\ell^2)^{\frac{1}{2}})\ \arctan(b/(a^2+\ell^2)^{\frac{1}{2}})\ ]$$

Here b is the length of the isothermal sidewall region and a is the height of the sidewalls.

The necessary integration in the above equation is best done numerically. The resulting longitudinal profiles of radiative flux along the central axis of the base of the U channel are shown in Figure 26.

Figure 26 shows calculated results for a high and a low air inflow velocity. The flux distributions are shown superimposed on a cross-sectional plane through the central axis of the base of the U channel; the starting point at the left of the Figure corresponds to the point where the surface temperature first reaches its maximum value and the distributions stretch downstream from that point. Also shown in the Figure are the integrals of the areas under these profiles which measure the total heat transferred to the wood by each mode per unit width of the wall. It is immediately clear that conduction heat transfer downstream through the wood is a minor contributor to the overall wood heat-up process. This helps explain how the two different kinds of wood, with their differing thermal conductivities, can have essentially the same smolder propagation velocity. One has to be more cautious in assessing the relative importance of the other two heat transfer modes; there are significant approximations in these numbers which are difficult to quantify. It is probable that both convection and conduction have been somewhat overestimated, given the assumptions noted above. It is probably reasonable to conclude that radiation is dominant at low flow velocities and that the two modes are comparable at high flow velocities. This is not necessarily what one might expect, however, and this issue is worth revisiting when more solid data are available on surface and gas temperatures in the U channel. This issue is worth pursuing because it makes inferences about other configurations and sample dimensions possible. For example, if radiation is the dominant heat transfer mode, to a first approximation, smolder will propagate just as fast against the air flow as with it. These issues will be examined in future tests.

3.7 Gas Phase Pyrolysis and Oxidation Kinetics

A further goal of the present study is to estimate the conditions of temperature, time and oxygen level required to destroy the various species evolved from wood burning. Such results could give the wood stove designer

target conditions which his design must shoot for in order to assure minimal air pollution.

Attempt at direct measurement. The original intent in this study was to perform experimental measurements of the rates of gas phase thermal pyrolysis and oxidation for about half a dozen of the species most prominent in the cold trap condensate. A laminar flow reactor was constructed for this purpose; such devices are relatively simple and inexpensive, which probably accounts for their continuing popularity for making measurements such as those planned here. Such reactors are typically constructed of small diameter tubes (in the present case, 1 mm and 2 mm ID) to assure good temperature uniformity over the tube cross section (this is necessary with highly exothermic oxidation reactions). The tube surface is heated uniformly to some desired temperature and the gas mixture of interest is passed through the tube at a measured flow rate so that the residence time is well-defined. The composition of the products leaving the reactor is then analyzed; from various series of such experiments one can infer the kinetic rate parameters for the degradation of the compound of interest.

Since the reactor tube is small in diameter, the gas molecules have a significant probability of striking the wall one or more times during their passage through the tube. In order to minimize the probability that such wall collisions would result in catalysis, the wall was made from pure gold, a material noted for its inertness in many contexts. When it became apparent that the wall was in fact causing heterogeneous reactions despite the use of gold, the reactor was designed to accept two different diameters of tube so that, in principle, the homogeneous and heterogeneous contributions to a measured net change in the concentration of the species of interest could be separated; only the homogeneous contribution is pertinent to the present study. Further tests with this double tube reactor revealed unexpected complexity, however: pyrolytic reactions appeared to be accelerated by the wall while oxidative reactions were retarded. This raised the question of the separability of the two modes of reaction (wall vs. gas phase); it was quite possible that they were interacting in a non-linear manner. In view of these complications , the limited time and the availability of an alternative means

to estimate the kinetic rate parameters, this experimental effort was terminated.

Prediction of the rate parameters. The rate of disappearance of a chemical species in an isothermal, well-mixed system containing oxygen is the result of two parallel modes of chemical change, thermal pyrolysis and oxidative attack. The first process is unimolecular under the conditions here and thus depends only on the concentration of the species of interest. The second process is potentially the result of attack by a variety of radical species on the target molecule and there are, therefore, several further parallel paths that depend both on the concentration of the target molecule and on the concentration of the attacking radical (bimolecular reactions). Thus one can write for the net rate of disappearance of the target molecule:

$$d[M]/dt = -k_u[M] - [M]\sum_i k_{b\,i}[R_i]$$

where [M] is the concentration of the target molecule (mol/liter), t is time, k_u is the rate constant for unimolecular decomposition, $k_{b\,i}$ is the rate constant for the i^{th} reaction that involves attack by radical R_i. Rearranging this slightly, one sees that the rate of disappearance of the target molecule is characterized by a time constant τ expressed as follows:

$$\tau = 1/\{k_u + \sum_i k_{b\,i}[R_i]\}$$

In an isothermal flow, this is the time for the concentration of the target molecule to decay to 1/e of its initial value. In the absence of oxygen, only the first term in the denominator applies since only unimolecular decomposition occurs. In the presence of oxygen both terms apply.
For the present purpose of estimating the rate of disappearance of pollutant species in the gas phase of a wood burning stove, one can assume that the principal oxidizing radical in all cases is the hydroxyl radical [29, 30]. One then needs an expression for the concentration of this radical as a

function of temperature. The following applies within about a factor of three for a wide range of fuel-air mixture ratios [30]:

$$[OH] = 10^{-1.7}\exp(-17600/T) \qquad \text{(mol/liter)}$$

where T is the absolute temperature in Kelvins. This is an equilibrium value of OH concentration established by various rapid elementary reactions in the radical pool.

In order to proceed further and estimate the net rate of target molecule disappearance, one needs estimates also for the rate constants. Data for k_u and k_{bi} were obtained from the literature or were developed by estimation techniques described in Appendix A of this report. These data are summarized for the selected compounds reported in Table 2. The species there include several identified in our previous study together with a selection of relevant aromatic species. For each chemical compound, the selected values for the rate constants, k_u and k_{bi}, together with computed values for $(OH)_{EQ}$ were incorporated into the above equations to develop values for τ. These computed values for each selected compound are shown in Figure 27, in which the predicted time-temperature degradation behavior of these compounds is illustrated for 63% decomposition, the so-called "1/e" degree of degradation. Corresponding degradation behavior for any other degree of decomposition can be obtained by recomputing τ for each temperature for pyrolysis or oxidation according to the expression,

$$\tau = k^{-1}\ln(1/(1-a))$$

In the equation above, a is the degree of decomposition which can be specified by dividing the percent of decomposition by 100.

Figure 27 shows separately the temperature-dependent time to destroy a target molecule by either pyrolysis or oxidation. Note that the requisite oxidation conditions for all of the species fall within a band that is about one order of magnitude wide; the pyrolysis conditions vary much more widely with the

chemical identity of the species. Except at high temperatures, oxidation is predicted to be the primary path of destruction.

Also indicated in Figure 27 is the approximate domain of time and temperature in which one can expect typical woodburning stoves to operate if the air supply is somewhat restricted. The upper temperatures certainly include flaming combustion; the lowest temperatures pertain to the pure smoldering mode examined in this study. The residence times are estimated from stove volume and typical air flow rates. It is worth noting that for this range of residence times the predicted temperatures necessary to oxidize the various pollutant species are in approximate agreement with the rule of thumb sometimes used by stove designers (1100°F ≃ 870 K; ref. 31).

It should be quite clear from Figure 27 that the temperature-time domain of operation of a wood stove, especially in the smoldering mode, is far from that necessary for effective destruction of the pollutant species generated by the wood burning process. On this Figure, the only realistic way to move in order to achieve pollutant destruction is upward in temperature, since the horizontal scale is logarithmic. To do this one needs to get all of the gas in the stove essentially up to the same temperature as the actively oxidizing char surface. With the usual random arrangement of wood logs in the firebox, there is simply not enough contact between the gas and the solid phases to approach this thermal equilibrium. Such contact requires re-sizing of the fuel down to small chunks, forming a packed bed through which all of the incoming air flow must pass. However, there are problems with using a packed bed fuel configuration. If the air moves through the bed in the same direction as the propagating smolder oxidation zone (forward smolder), the gases must pass through cooler regions of the fuel bed where they will emerge contaminated with pyrolysis vapors. If the air moves in the opposite direction (reverse smolder), there is a tendency for the smolder reaction zone to be incomplete in its consumption of the solid [7]. Pre-heating the air is of some help in boosting the emerging gas temperature [31], but extensive pre-heating requires significant re-design of the woodstove.

The conclusion which the preceding discussion rather insistently points to is that effective elimination of pollutants generated in a woodstove operated in a smoldering mode requires either some drastic re-design of the stove (not envisioned above) or the use of some form of afterburner on the exhaust. Given the large gap in Figure 27 between the typical operating conditions for smoldering and the estimated requisite conditions for pollutant destruction, it is unlikely that refinements in the estimates of the latter would alter this conclusion.

3.8 Conclusions

In the apparatus used here, the forward spread of smolder over solid wood was self-sustaining only over a rather narrow range of air inflow rates. The lower limit is probably extendable by further thermal insulation around the sample and/or by the use of thicker wood; the upper limit, due to the transition to flaming, is probably more inherent in the behavior of wood and thus is probably independent of the apparatus design.

Both red oak and white pine behave in a similar manner in this forward smolder mode and it appears that the smolder process tends to sweep out a constant volume of wood as a function of time, independent of the wood properties. The minor role for heat conduction through the wood in causing smolder to propagate is one reason for this; the equal temperatures achieved on the oxidizing char surface is the other. The latter fact evidently reflects equal amounts of heat evolved per gram of oxygen reaching the char surface of either wood. The essentially linear increase in smolder velocity, surface temperature, rate of heat and product release with increases in air inflow rate also reflect a pivotal role for the rate of oxygen supply to the oxidizing char surface. However, the failure of the char oxidation zone to grow to the point where it was long enough to consume all incoming oxygen implies that oxygen supply rate has a less than total control over the rate of smolder propagation. This is in contrast to the complete dominance oxygen supply rate has in one-dimensional forward smolder through a packed fuel bed. In the present configuration, the failure to consume all oxygen points to a key role for downstream heat transfer rate in the propagation process. This

heat transfer was seen to be dominated by radiation, at least at low air flow rates; at higher flow rates convection appears to be equally important.

The major products of the wood smolder process appear to be essentially the same here, in the previous forced gasification experiments and in a wood stove operated in a smoldering mode. The ratio of CO to CO_2 does vary among these various gasification circumstances and this appears to reflect varying degrees of CO oxidation. This oxidation appears to be the only significant change that occurs to the products evolved from smoldering wood as they pass through a wood stove. Estimates of the kinetic rate parameters for the oxidation and pyrolysis of several of the species in the tar confirm that they are not subject to destruction at the combination of temperatures and times encountered in conventional wood stoves. Gas phase destruction is possible only at higher temperatures and these are probably achievable only through thee use of an auxiliary heat source such as an afterburner, if a stove is to be operated in a smoldering mode.

Acknowledgements

Mr. Scott Dolan provided extensive assistance in setting up and performing the experiments as well as in the chromatographic analyses. This work was supported in part by the Department of Energy, Office of Buildings and Community Systems, under Contract No. DE-AI01-76PRO6010.

REFERENCES

[1] Ohlemiller, T., Kashiwagi, T. and Werner, K., "Products of Wood Gasification", National Bureau of Standards NBSIR 85-3127, April 1985.

[2] Ohlemiller, T. and Rogers, F., "Smoldering Combustion Studies of Rigid Cellular Plastics", Princeton University Department of Mechanical and Aerospace Engineering Report No. 1432, May, 1979 (Final report to the Products Research Committee).

[3] Thring, M. W., The Science of Flames and Furnaces, Chapman and Hall , London (1952) p. 134 ff.

[4] Spalding, D., Some Fundamentals of Combustion, Butterworths, London (1955) p. 98 ff.

[5] Palmer, K., Combust. Flame 1, (1957) 129.

[6] Ohlemiller, T., "Forced Smolder Propagation and the Transition to Flaming in Cellulosic Insulation", National Bureau of Standards NBSIR 85-3212, October 1985.

[7] Ohlemiller, T. and Lucca, D., Combust. Flame 54, (1983) 131.

[8] Zabetakis, M.,"Flammability Characteristics of Combustible Gases and Vapors", Bureau of Mines Bulletin 627 (1965).

[9] Alexopoulos, S. and Drysdale, D., University of Edinburgh, private communication, 1987.

[10] Cooke, M., Allen, J., and Hall, R., "Characterization of Emissions from Residential Wood Combustion Sources", in Residential Solid Fuels, Environmental Impacts and Solutions, Cooper, J. and Malek, D. (editors), Oregon Graduate Center, Beaverton, Oregon (1982), 139.

[11] Anon., "Residential Wood Heater Test Report", Phase II, Volume I, Tennessee Valley Authority, Energy Use Test Facility, CHattanooga, Tenn., August 1983.

[12] Tillman D., Rossi, A.,and Kitto, W., Wood Combustion; Principles Processes and Economics, Academic Press, New York (1981), p.43.

[13] Magnani, C. and Farouq-Ali, S., Soc. Petroleum Eng. J., October, 1975, p.425.

[14] Krukovskii, V., Pitin, R. and Farberov, I., "Underground Processing of Fuels", translated from Russian and published by the Israel Program for Scientific Translations, Jerusalem ,Israel (1963), p. 91 ; available from the Federal Scientific and Technical Information Clearinghouse, Washington, D.C.

[15] Roberts, A. and Clough, G., Combust. Flame 11, (1967), p.365.

[16] Dryer, F., "High temperature oxidation of carbon monoxide and methane in a turbulent flow reactor", Princeton University Aerospace and Mechanical Sciences Dept. Report No. T-1034 (1972).

[17] Laurendeau, N., Prog. Energy Combust. Sci. 4, (1978), p. 221.

[18] Kashiwagi. T., Ohlemiller, T. and Werner, K., Combust. Flame 69, (1987), p. 331.

[19] Ahmed, S. and Beck, M., Carbon 23, (1985), p.513.

[20] Degroot, W. and Shafizadeh, F., Carbon 21, (1983), p.61.

[21] Shafizadeh, F., Bradbury, A., Degroot, W. and Aanerud, T., Ind. Eng. Chem., Prod. Res.Dev. 21, (1982) p.97.

[22] Boroson, M., "Secondary reactions of tars from pyrolysis of sweet gum

hardwood", Ph. D. thesis, Dept. of Chemical Engineering Massachusetts Institute of Technology, May, 1987.

[23] Gann, R., "Comparison of principal combustion products from a wood stove as a function of height in the chimney", Fiscal Year 1982 Final Report from the National Bureau of Standards on DOE Project No. 133a,DE-A01 -76PR06010, October 1982.

[24] Muhlbaier, J., "A characterization of emissions from wood-burning fireplaces", in Residential Solid Fuels, ibid, p.164.

[25] McCaffrey, B., "Purely Buoyant Diffusion Flames: Some Experimental Results", National Bureau of Standards NBSIR 79-1910, October 1979.

[26] Huggett, C., Fire and Materials 4, (1980), p.61.

[27] Kanury, A. and Blackshear, P., Combust. Sci. Technol. 1, (1970), p.339.

[28] Eckert, E. and Drake, R., Analysis of Heat and Mass Transfer, McGraw-Hill, New York, (1972), p.622.

[29] Benson, S. Twenty-First Symposium (International) on Combustion (1986), proceedings in press.

[30] Tsang, W. and Shaub, W., "Chemical processes in the incineration of hazardous materials", in Detoxication of Hazardous Waste, (J. Exner, ed.), Ann Arbor Science, Ann Arbor Michigan (1982), p.41.

[31] Dobson, L., "High-tech non-catalytic woodstove design considerations", in Proceedings of the International Conference on Residential Wood Energy, Reno, Nevada, March, 1986.

TABLE 1

Normalized Area Percentage of Some Tar Components*

Component	From White Pine			From Red Oak		
TEST:	FG**	SWS 16	SWS 13	FG**	SWS 18	SWS 17
Furaldehyde	0.35	1.67	1.59	16.8	10.7	10.5
Phenol	0.70	0.14	0.28	0.78	0.69	1.1
Guaiacol	0.54	0.90	0.81	0.82	2.19	2.23
Creosol	1.00	1.00	1.00	1.00	1.00	1.00
Acetic Acid	--	1.06	--	17.3	18.8	7.76
Isoeugenol	0.64	0.14	0.56	0.66	0.21	0.26
Furfuryl Alcohol	0.33	0.24	0.47	2.59	0.75	1.34
Toluene	1.43	0.81	1.73	1.82	0.54	1.33

*The area percentages are computed relative to the total area of all peaks eluted from the chromatograph (minus ethanol and methanol); note, however, that in Ref. 1 it was concluded that only about 20% by weight of injected tar is eluted.

**FG signifies the base case test conditions of forced gasification from Ref. 1.

TABLE 2: Summary of Rate Constant Data

Compound (i)	#	$\simeq k_u$* (sec^{-1})	$\simeq k_{bi}$ ($T \gtrsim 300°C[573°K]$) ($L \cdot mol^{-1} \cdot sec^{-1}$)
benzene	1	$5.75 \times 10^{16} \exp(-58400/T)$	$1.96 \times 10^3 T^2 \exp(-344/T)$
toluene	2	$3.16 \times 10^{15} \exp(-44400/T)$	$4.57 \times 10^3 T^2 \exp(+11/T)$
phenol	3	$3.16 \times 10^{15} \exp(-43500/T)$	$1.81 \times 10^3 T^2 \exp(-100/T)$
o-xylene	4	$2k_u(2)$	$1.05 \times 10^4 T^2 \exp(-35/T)$
m-xylene	5	$k_u(4)$	$1.03 \times 10^4 T^2 \exp(-127/T)$
p-xylene	6	$k_u(4)$	$1.05 \times 10^4 T^2 \exp(-99/T)$
naphthalene	7	$1.33k_u(1)$	$6.75 \times 10^3 T^2 \exp(-969/T)$
phenanthrene	8	$1.67k_u(1)$	$4.97 \times 10^3 T^2 \exp(-1000/T)$
anthracene	9	$1.67k_u(1)$	$6.63 \times 10^3 T^2 \exp(-1000/T)$
biphenyl	10	$1.67k_u(1)$	$3.92X10^3 T^2 \exp(-1000/T)$
benzo(a)pyrene	11	$1.83k_u(1)$	$5.66 \times 10^3 T^2 \exp(-1000/T)$
2-methyl-naphthalene	12	$k_u(2)$	$3.31 \times 10^4 T^2 \exp(-100/T)$
2,3-dimethyl-naphthalene	13	$2k_u(2)$	$4.88 \times 10^4 T^2 \exp(-100/T)$
o-cresol	14	$k_u(2)+k_u(3)$	$2.53 \times 10^4 T^2 \exp(-100/T)$
m-cresol	15	$k_u(14)$	$3.61 \times 10^4 T^2 \exp(-100/T)$
p-cresol	16	$k_u(14)$	$2.77 \times 10^4 T^2 \exp(-100/T)$
benzaldehyde	17	$10^{16} \exp(-44000/T)$	$1.02 \times 10^4 \exp(-100/T)$
furfural	18	$3.16 \times 10^{15} \exp(-36400/T)$	$k_{bi}(17)$
furfuryl alcohol	19	$3.16 \times 10^{15} \exp(-38700/T)$	$k_{bi}(4)$
creosol	20	$1.17 \times 10^{16} \exp(-33100/T)$	$3.98 \times 10^4 T^2 \exp(-100/T)$
vanillin	21	$k_u(20)$	$6.63 \times 10^3 T^2 \exp(-100/T)$

*Numbers in parentheses refer to the compound with that number; thus $k_u(1)$ means the value of k_u for compound 1.

APPENDIX A

ESTIMATION OF KINETIC RATE CONSTANTS

Rate constants, k_u and K_{bi}, were either determined from literature reports or developed by estimation methods for the twenty one organic compounds listed in Table 2 of the main report. The details of the development of these data are described below. It is unlikely that errors in estimating k_u and k_{bi} would lead to conclusions contrary to those developed in this report. An order of magnitude error in estimating the rate constants would not result in a corresponding shift in the time-temperature curves, such that they would overlap the smoldering wood-burning stove domain illustrated in Figure 27 of the main report. Care should of course be exercised in utilizing the estimated rate constants for purposes other than that intended in this study.

Rate Constant Development:

1. Benzene

Rate constants for both k_u and k_{bi} have been reported in the literature for the temperature domain of interest (1,2). These reported values are used without modification.

2. Toluene

Rate constants for both k_u and k_{bi} have been reported in the literature for the temperature domain of interest (2,3). These values are used without modification.

3. Phenol

A rate constant for k_u has been reported in the literature (4). This value is used without modification. Atkinson (2) has reported a value for k_{bi} at 298 K (2.83×10^{-11} $cm^3 \cdot molec^{-1} \cdot sec^{-1}$). The low temperature mechanism is dominated by an addition reaction to form a complex which can either decompose back to the original reactants or stabilize. At higher temperatures additional reactions

are possible, e.g., metathesis (hydrogen abstraction) or elimination (displacement of hydrogen). Available evidence, based on other reaction systems appears to favor the metathesis reaction (see for example the work of Madronich and Felder (5). Examination of rate constants for hydroxyl radical reaction with other substituted benzene compounds (2) at T=298 K and at T=1000 K (e.g., data for toluene, o-xylene, m-xylene, p-xylene (2)) suggests that $k_{bi}(1000)/k_{bi}(298)$ has a value of the order of 1 and that E_a/R has a value of the order of 100 K. Using these suggested relationships based upon examination of literature data, and Atkinson's formulation for an expression describing the temperature dependence of k_{bi}, $(AT^2\exp(-b/T))$, it can be shown that $k_{bi} \simeq (3.0 \times 10^{-17} \exp(-100/T) \times T^2))$ $cm^3 \cdot molec^{-1} \cdot sec^{-1}$ is an estimate for reaction of hydroxyl radical with phenol at higher temperatures than about 450 K. The lower temperature cutoff is approximate and reflects the complex nature of the reaction mechanism at intermediate temperatures (2).

4. o-, m-, and p-xylene

An estimate for k_u for these compounds is that k_u is about twice that reported for toluene, since, in the former cases, each compound has two methyl group substituents and, in the latter case, toluene has one methyl substituent. Rate constants for k_{bi} for each compound have been reported in the literature (2). These values are used without modification.

5. Naphthalene

An estimate for k_u for naphthalene is that k_u is $\simeq 1.3 \times k_u$(benzene). The rough adjustment is to allow for the differing number of hydrogen atoms. More refined estimates are possible but are unnecessary for the purposes of this study. A rate constant for k_{bi} has been reported in the literature (2) and is used without modification.

6. Phenanthrene

An estimate for phenanthrene is that $k_u \simeq 1.67 k_u$(benzene). The adjustment

follows the reasoning given for estimation of k_u(naphthalene). A rough estimate for k_{bi} can be made as follows:

Using reported ionization potentials for benzene (IP=9.24 eV) and napthalene (I=8.15 eV) (6) plus k_{bi} values for these compounds for at T=1000 K (2,7), a plot of $\log_{10} k_{bi}$(1000 K) versus IP can be constructed. It has been observed (2) that such linear plots result for homogeneous series of compounds. Then using the reported value of IP=7.86 eV (7) for phenanthrene, an estimated value for k_{bi}(1000 K) for phenanthrene can be derived from such a plot. This is found to be $k_{bi}=4.99\times10^{-12}$ $cm^3 \cdot molec^{-1} \cdot sec^{-1}$. For unsubstituted aromatic compounds it appears that as an estimate, $E/R \simeq 1000$ K, and using a fitting function (2) of $AT^2e^{-b/T}$, a value for A can be found, $A=8.25\times10^{-18}$ $cm^3 \cdot molec^{-1} \cdot sec^{-1} \cdot deg^{-2}$. The rate constant expression that can be constructed from this analysis (see Table 2 of main text) can be used to check the literature value reported for k_{bi} (phenanthrene) at T=748 K (2.2×10^{-2} $cm^3 \cdot molec^{-1} \cdot sec^{-1}$(2). The calculated value found from the estimated expression is found to agree well with the literature value, the former being found to be k_{bi}(phenanthrene, estimated)$=2.4\times10^{-12}$ $cm^3 \cdot molec^{-1} \cdot sec^{-1}$. The estimated expression for k_{bi} was assumed useful without modification for $T \gtrsim 600$ K. Below this approximate temperature range, competition with other reaction channels causes increasing uncertainties in the use of this expression.

7. Anthracene

An estimate for anthracene is the k_u is $\simeq 1.67 k_u$(benzene). The adjustment follows the reasoning given for estimation of k_u(naphthalene). A value for k_{bi} has been estimated according to the method outlined for phenanthrene. In making this estimate a value of IP=7.41 eV was used for anthracene (6).

8. Biphenyl

An estimate for biphenyl is that k_u is $\simeq 1.67 k_u$(benzene). The adjustment follows the reasoning given for estimation of k_u(naphthalene). A value for k_{bi} has been estimated according to the method outlined for phenanthrene. In

making this estimate a value of IP=8.27 eV was used for the biphenyl molecule (6).

9. Benzo(a)pyrene

An estimate for benzo(a)pyrene is that k_u is $\simeq 1.83 k_u$(benzene). The adjustment follows the reasoning given for estimation of k_u(naphthalene). A value for k_{bi} has been estimated according to the method outlined for phenanthrene. In making this estimate a value of 7.63 eV was used for the IP of benzo(a)pyrene (6). The value required for k_{bi} at T=298 K which is required in the calculation method outlined above was obtained from a plot of $\log_{10} k_{bi}$ at T=298K versus IP for benzene and naphthalene, resulting in a value at T=298 K of k_{bi}(benzo(a)pyrene) = 3.16×10^{-11} $cm^3 \cdot molec^{-1} \cdot sec^{-1}$. The IP used for benzo(a)pyrene in the calculations is an average of three reported values: 7.56, 7.60 and 7.73 eV (6).

10. 2-methyl naphthalene

An estimated value for k_u is $k_u \simeq k_u$(toluene), since both compounds have one methyl group from which a hydrogen atom can be eliminated. A value for k_{bi} was derived using the reasoning applied in developing a value for k_{bi}(phenol). In making the estimate, a value of k_{bi}(2-methyl naphthalene)= 5.23×10^{-11} $cm^3 \cdot molec^{-1} \cdot sec^{-1}$ at T=295 K was utilized (2).

11. 2,3-dimethyl naphthalene

An estimated value for k_u is $k_u \simeq 2k_u$(toluene). The reasoning for this estimate follows that for o-xylene. A value for k_{bi} was derived using the reasoning applied in developing a value for k_{bi}(phenol). In making the estimate a value of k_{bi}(2,3-dimethyl naphthalene)= $7.68 \times 10^{-11} \cdot cm^3 \cdot molec^{-1}$ sec^{-1} at T=295 K was utilized (2).

12. o-, m-, p-cresol

Since the cresols each have one methyl and one hydroxyl substituent groups having approximately comparable elimination rate constants, following the reasoning applied to the xylenes, an estimated value of k_u for the cresols is $k_u \simeq k_u(\text{toluene}) + k_u(\text{phenol})$. Estimated values for k_{bi} were derived using the reasoning applied in developing a value for $k_{bi}(\text{phenol})$. In making the estimates for k_{bi} at T=298 K, the values used were 4.0×10^{-11}, 5.7×10^{-11} and 4.4×10^{-11} respectively for the ortho-, meta- and para-cresol isomers (2).

13. Benzaldehyde

The activation energy for k_u can be estimated from a calculation of heat of reaction estimated from thermodynamic parameters abstracted from the literature (3,8) in which it is assumed that a hydrogen atom is eliminated from the formyl substituent rather than from the aromatic ring. This pathway is favored by the formation of the resulting resonance stabilized radical (9). A pre-exponential factor of 10^{+16} sec^{-1} is estimated (13). An estimated value for k_{bi} was derived using the reasoning applied in developing a value for $k_{bi}(\text{phenol})$. In making the estimate a value for k_{bi} of 1.6×10^{-11} $cm^3 \cdot molec^{-1} \cdot sec^{-1}$ at T=298 K was used (10).

14. Furfural

An approximate lower limit for the activation energy for k_u was estimated by first examining differences in the heats of reaction calculated (3,8) for elimination of OH from $(CH_3)OH$ and the compound $(C_6H_5)CH_2OH$, respectively. The difference in heats of reaction was taken as an approximate aromatic ring stabilization energy correction factor. This correction factor (also derivable from comparison of methane and toluene) was applied to an estimated heat of reaction for hydrogen atom elimination from formaldehyde to obtain the activation energy for hydrogen atom elimination from the formyl group substituent in furfural. This activation energy may be an underestimate, a higher value being derived assuming E_a for $k_u(\text{furfural})$ is equal to the activation energy associated with the unimolecular dissociation of benzaldehyde. Again, however, this difference in estimates has no effect upon the possibility of overlap in the time-temperature curves shown in Figure 27 and discussed in this report. The pre-exponential factor was assumed to be

slightly less for furfural than for benzaldehyde (5). An approximate estimate for k_{bi}(furfural) is that it is approximately equal to k_{bi}(benzaldehyde), the two molecules having the same substituent group attached.

15. Furfuryl alcohol

The activation energy for k_u was assumed comparable to the activation energy for hydroxyl radical elimination from $(C_6H_5)CH_2OH$. For the latter reaction, the bond dissociation energy is about 77 kcal per mole (8). The pre-exponential factor was set similarly to that for furfural. The bimolecular rate constant was assumed equivalent to that for phenol by analogy to the comparison between k_{bi} for benzaldehyde and furfural.

16. Creosol

The rate constant for k_u is assumed equivalent to that for the molecule $(C_6H_5)O\text{-}CH_3$ for the indicated carbon-oxygen bond rupture. The latter rate constant has been derived in a shock tube study (11). An estimated value for k_{bi} was derived using the reasoning applied in developing a value for k_{bi}(phenol). In making the k_{bi} estimate, a value for k_{bi}(creosol) at T=298 K had to be derived. This was calculated according to the procedural method developed and described by Zetzsch (10). As discussed in Atkinson's report, the rate constant can be expressed by Zetzsch's method as,

$$\log_{10} k_{bi}(298) = -11.64 - 1.31 \sum_1 \sigma_i^+$$

In the equation above, substituent constants, σ_i^+, are selected which produce the largest negative value for the substituent constant summation term, $\Sigma\sigma^+$. The values of σ^+ used for estimating k_{bi}(creosol) were taken from Zetzsch's paper except for σ^+ of the m-hydroxyl group, $\sigma^+ \simeq 0.01$, which was found by comparing values for σ^+ for m-, p-amino, p-hydroxy then interpolating between substituent values for the amino- and methoxy-group values using the known value of σ^+ for p-hydroxy (12).

17. Vanillin

The rate constant, k_u, for vanillin was assumed equivalent to that for creosol, the same bond undergoing rupture. An estimated value for k_{bi} was derived using the reasoning applied in developing a value for k_{bi}(phenol). As with creosol, in making the k_{bi} estimate, a value for k_{bi}(vanillin) at T=298 K had to be derived. As with creosol, Zetzsch's method was applied (2,10), with σ^+ substituent constants obtained from reports of Brown and Okamoto (12) and Zetzsch (10), except for σ^+ for the formyl substituent, $\simeq 0.46$, which was estimated by making comparisons, as was done for creosol.

REFERENCES, APPENDIX A

[1] Hsu, D.S.Y., Lin, C.Y. and Lin, M.-C., 20th Symposium (International) on Combustion, The Combustion Institute, Pittsburgh, PA, pp623-630 (1984).

[2] Atkinson, R., Chem. Rev. 85, 69-201 (1985); and references cited therein.

[3] Benson, S.W. and O'Neal, H.E., Kinetic Data on Gas Phase Unimolecular Reactions, NSRDS-NBS-21, National Bureau of Standards, Washington, D.C. (1970).

[4] Shaub, W.M. and Tsang, W., Environ. Sci. Tech. 17, 721-730 (1983).

[5] Madronich, S. and Felder, W., J. Phys. Chem. 89, 3556-3561 (1985).

[6] Rosenstock, H.M., Draxl, K., Steiner, B.W. and Herron, J.T., J. Phys. Chem. Ref. Data 6 (Suppl. No. 1), (1977).

[7] Biermann, H.W., MacLeod, H. Atkinson, R., Winer, A.M. and Pitts, J.N.Jr., Environ. Sci. Tech. 19, 244-248 (1985).

[8] Benson, S.W., Thermochemical Kinetics, John Wiley (1976).

[9] Stein, S.E., Center for Chemical Physics, NBS, private communication (1986).

[10] Zetzsch, C., Abstract A-11 (p29) in: 15th Informal Conf. on Photochemistry, Stanford, CA, June 27-July 1 (1982).

[11] Hsu, D.S.Y., private communication

[12] Brown, H.C. and Okamoto, Y., J. Amer. Chem. Soc. 80, 4979-4987 (1958).

[13] Tsang, W. and Shaub, W. in: Exner, J.H. (editor), Detoxication of Hazardous Waste, Ann Arbor Science, Ann Arbor (1982).

APPENDIX B

APPLYING SIMPLIFIED WOODSTOVE MODELS

Viewed as a chemical reactor, a wood stove is an extremely complex device. It turns two reactants, one fed batchwise (wood) and one fed continuously (air), into a two-phase mixture of hundreds of products (smoke). The interior of the reactor is characterized by poor mixing and sharp gradients in temperature and chemical reaction rates. Modeling this system so as to predict the rate of evolution of a given product is a task beyond the current state of the art, in the absence of drastic simplifying assumptions. Here the problem is briefly addressed in terms of the two simplest possible models of a chemical reactor, the isothermal plug flow reactor and the perfectly stirred reactor [1].

The isothermal plug flow reactor can be visualized as a simple tube along which the reactants flow as they are converted to products. The reactants are completely mixed and any heat they evolve as they react does not change the local temperature significantly. (If the reactor is adiabatic instead of isothermal, one has, in effect, a pre-mixed laminar flame.) Such a model is a very crude approximation of the behavior of the gas phase in a wood stove, especially since a plug flow path through the firebox is hard to identify. If, nevertheless, one wished to apply such a model to make some very rough estimates of product evolution rates, the results in this report and in the previous related report are of some use in this regard for the smoldering operation mode. Suppose that one has estimated, within an order of magnitude, the effective plug flow velocity and path length through the stove of interest. One then needs the concentration of wood gases which follow this path in accompaniment with the assigned air inflow rate. Figure 7 in the main body of the report gives the relation obtained here between the rate of air inflow and the rate of wood gasification. This applies strictly only to the configuration examined here but it should apply rather closely to a set of parallel channels subject to comparable air flow per channel; this provides a rough basis for applying this result to a less organized load of wood. One then has an estimate of the mixture of fuel and air entering the gas phase plug flow reactor.

Suppose that the component of interest is in the tar. Figures 20 and 21 give an estimate of the fraction of gasified wood which is tar; if the component is one of those identified in the previous work (ref. 1 in main body of this report), the data accompanying Figure 18 of that report (see also the discussion of that Figure) provide an estimate of the fraction of that component in the tar. Thus one has an estimate of the concentration of the component of interest entering the plug flow reactor.

To calculate the amount of this component which survives passage through this reactor requires that one pick a temperature for the reactor and then utilize the estimated kinetic rate parameters in Table 2 of the main body of this report. For the estimated time that the gas will spend at this temperature and the net pyrolytic and oxidative kinetic rate constant obtained from Table 2, one then gets the fraction of the species which is destroyed by plugging these numbers into the last equation in Section 3.7 and solving for the value of a.

A perfectly stirred reactor is another idealization of reality. Here it is assumed that the reactants mix instantly throughout the reactor volume; composition and temperature are thus uniform throughout. The reactants, on average, spend a time in the reactor equal to the reactor volume divided by the volumetric flow rate of the reactants. From a simple species balance one can show the change in the concentration of the reactant between entering and exiting the reactor is [1]:

$$\Delta Y = (V_R/F) \cdot RR(T)$$

Here ΔY is the change in mass fraction of the species of interest, V_R is the estimated volume of the gas phase in the well-stirred portion of the firebox, F is the mass flow rate of the reactants into the gas phase of the firebox and RR(T) is the volumetric rate of consumption of reactant mass, obtainable at any chosen temperature T from the rate data in Table 2. Thus the application of this simplified model, using the data developed in this study, is quite similar to that for the plug flow model.

References, Appendix B

[1] Smith, J., Chemical Engineering Kinetics, Second edition, McGraw-Hill Book Company, New York (1970), Chapter 3

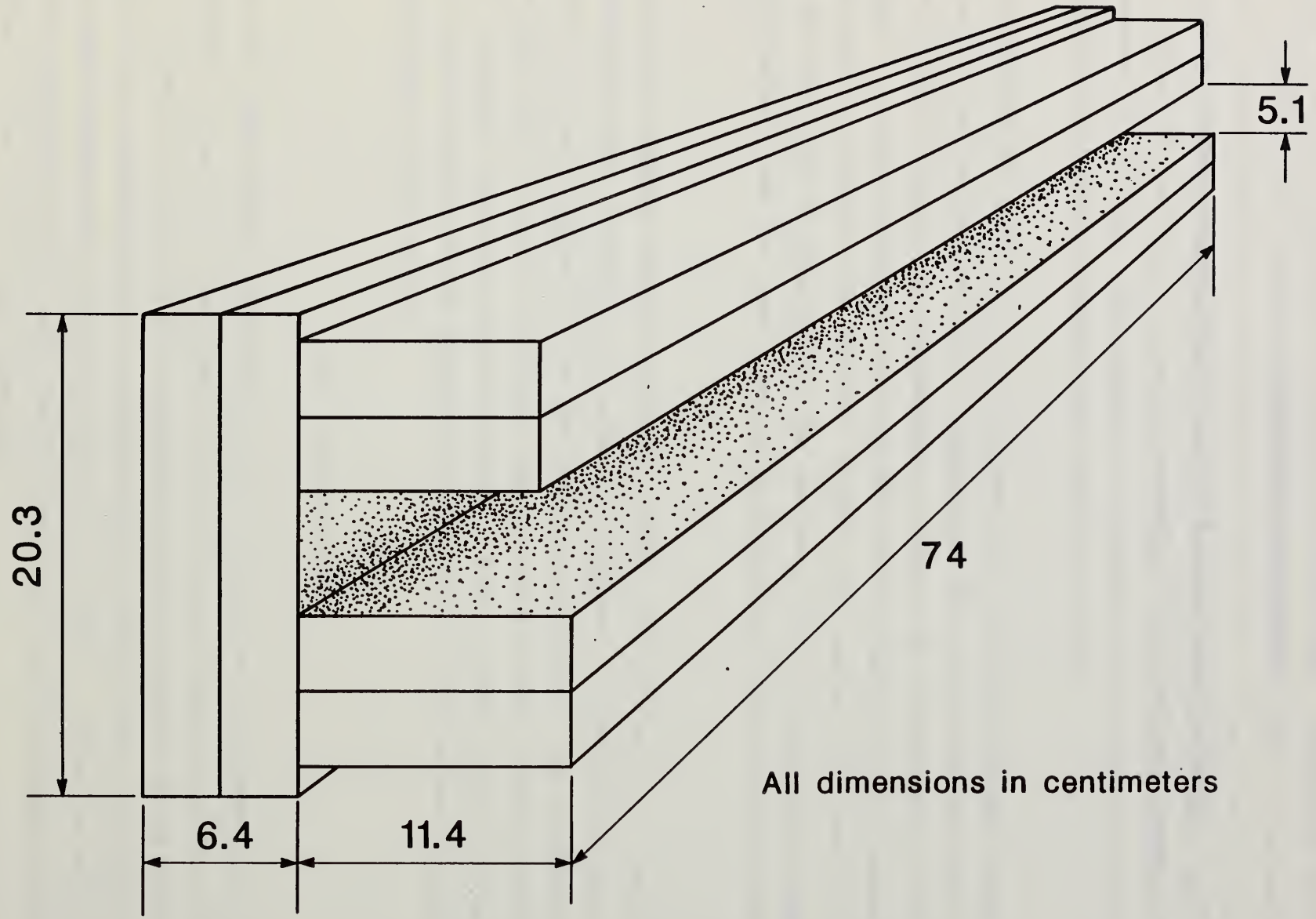

Figure 1. Wood sample configuration and dimensions. Actual orientation of sample in wood combustion chamber is same as that shown here.

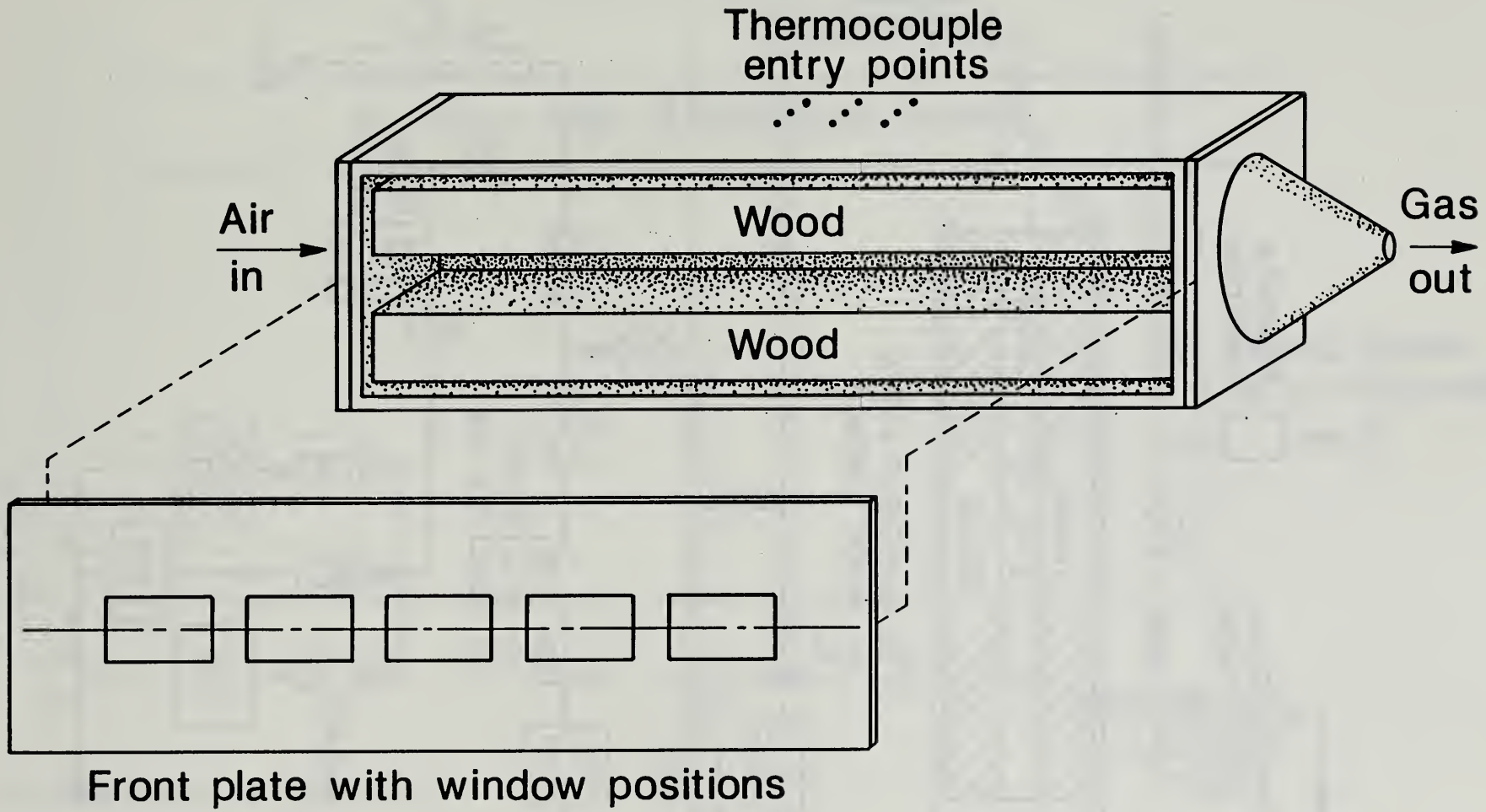

Figure 2. Schematic of wood combustion chamber with sample in place. Windows at indicated positions on front plate protrude outward away from the U-channel in the sample.

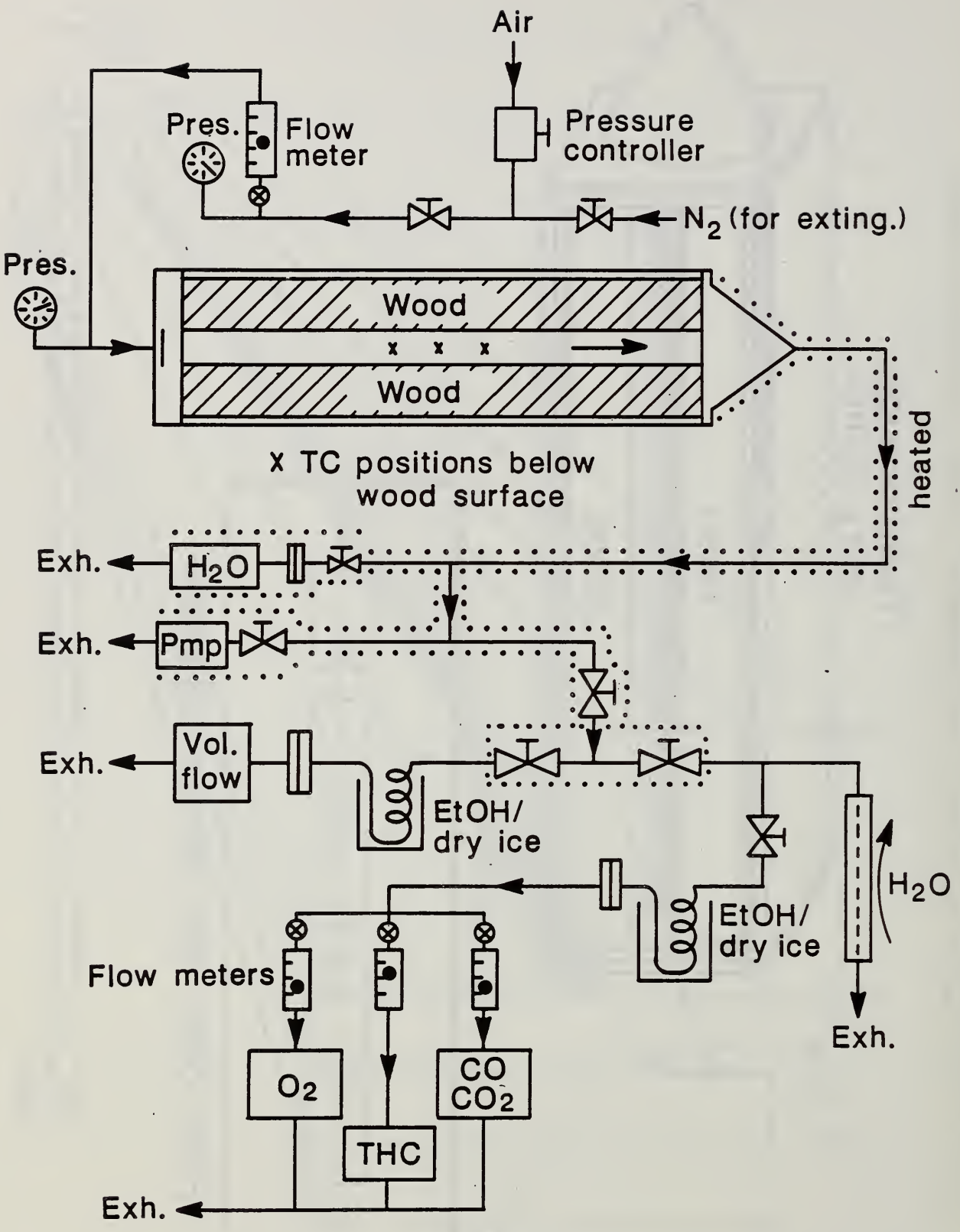

Figure 3. Schematic of flow system supporting the wood combustion chamber.

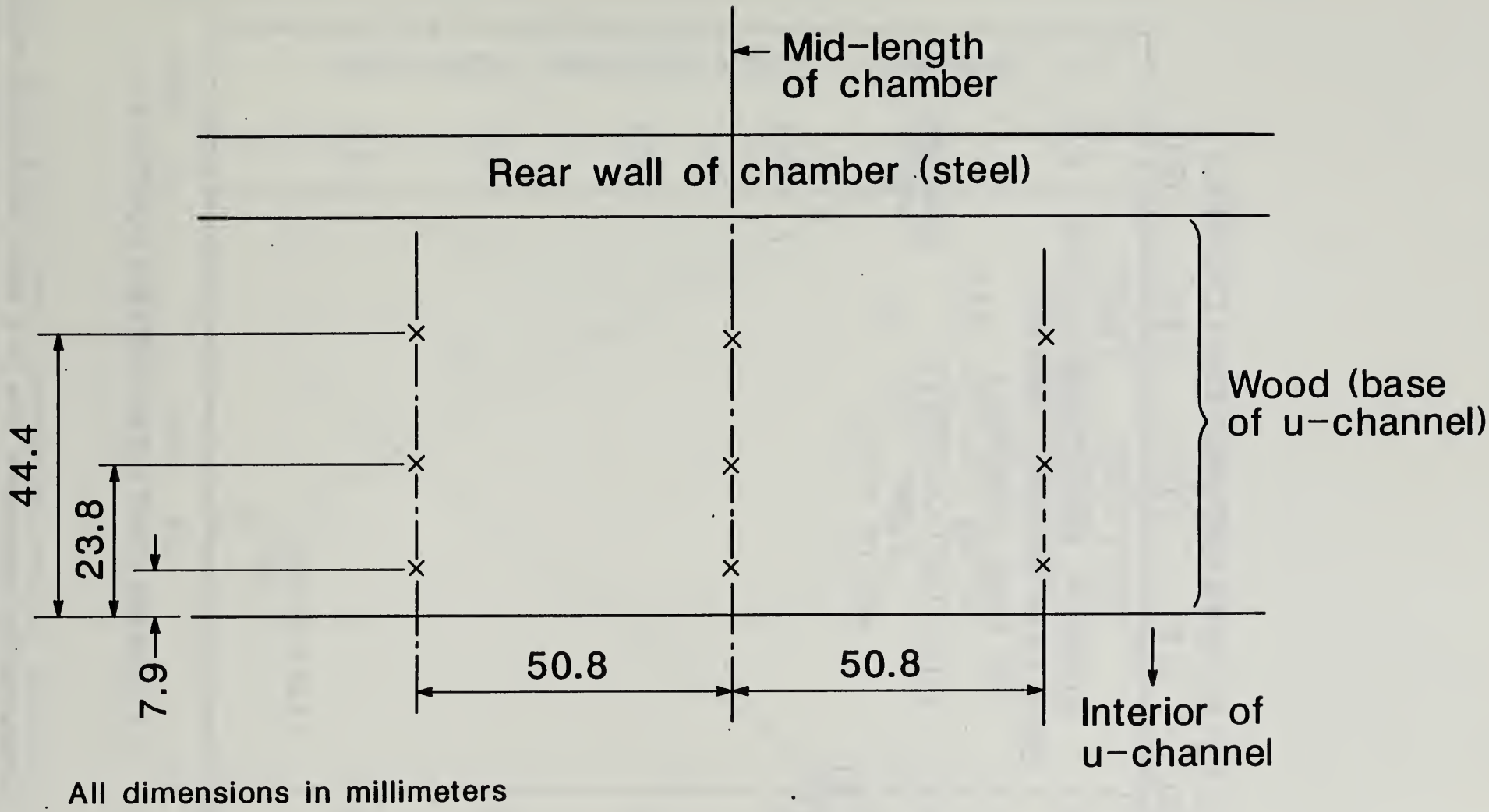

Figure 4. Arangement of thermocouple insertion points on the top side of the wood combustion chamber. These same spacings are assumed to hold at the actual depth of the thermocouple junctions.

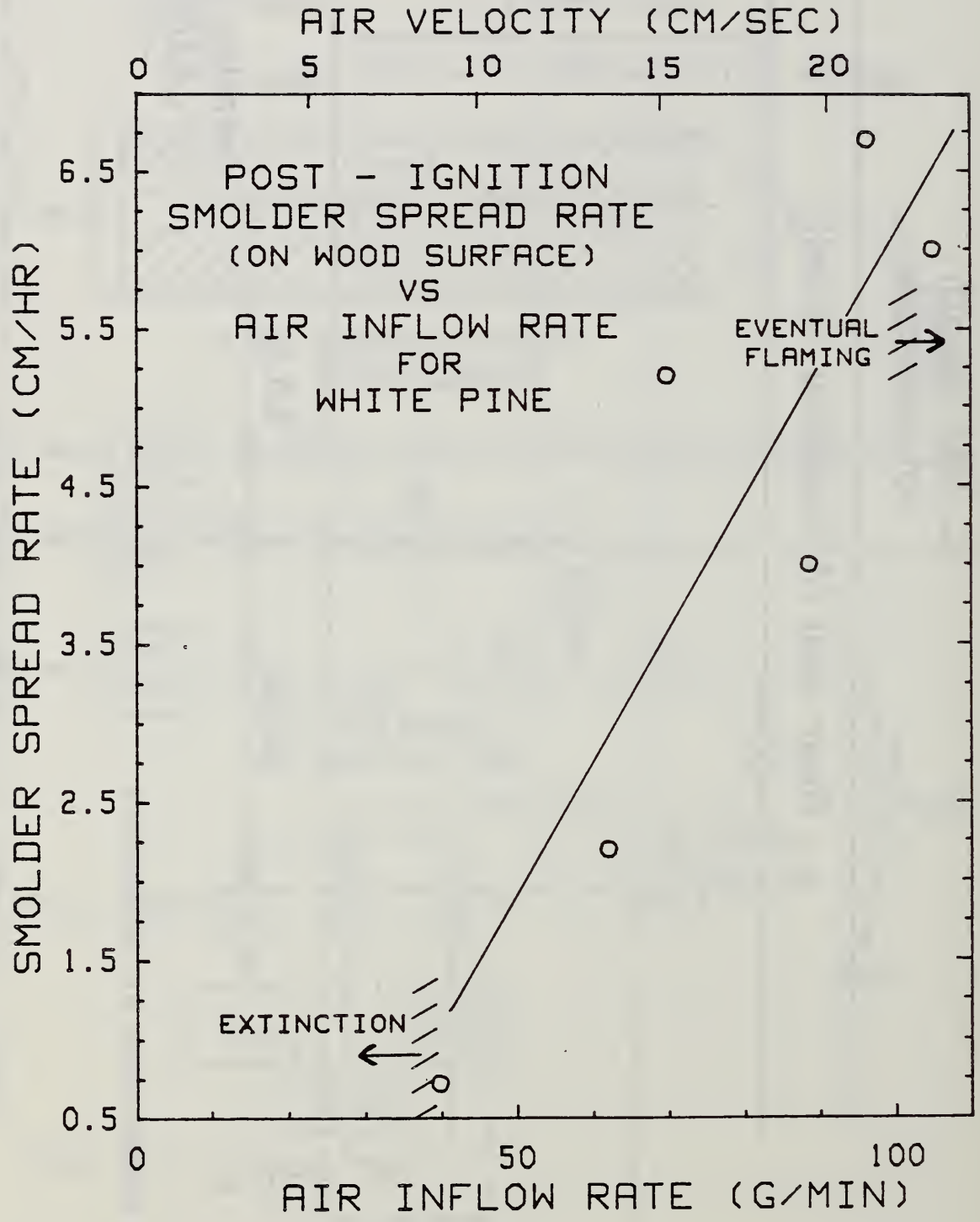

Figure 5(a). Post-ignition smolder propagation rate as a function of air flow along the U-channel for white pine. The cross-hatching indicates the approximate position of the borders for extinction and for flaming.

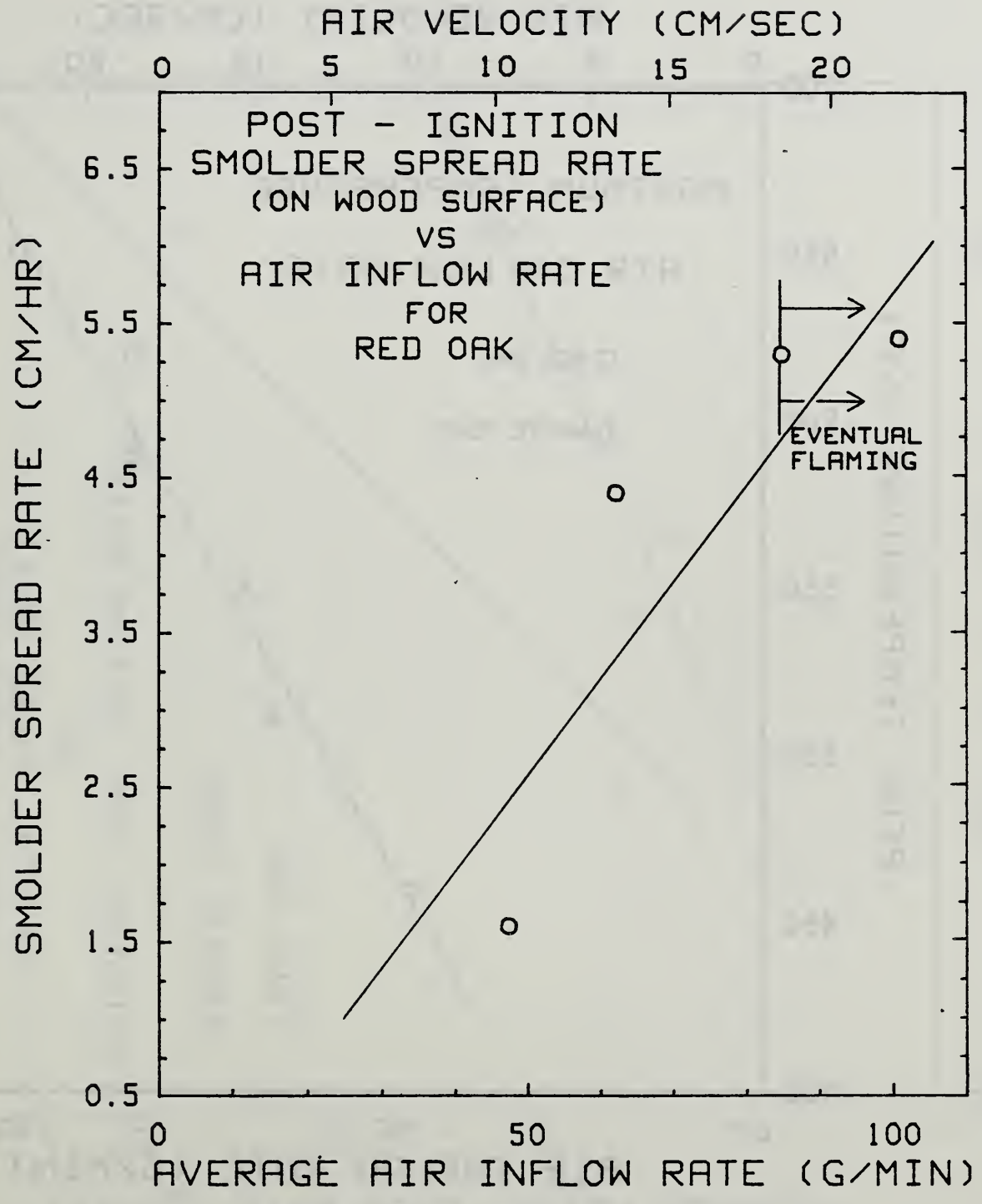

Figure 5(b). Post-ignition smolder propagation rate as a function of air flow along the U-channel for red oak. The line with the arrows indicates that in the two tests at or to the right of the line, flaming eventually developed.

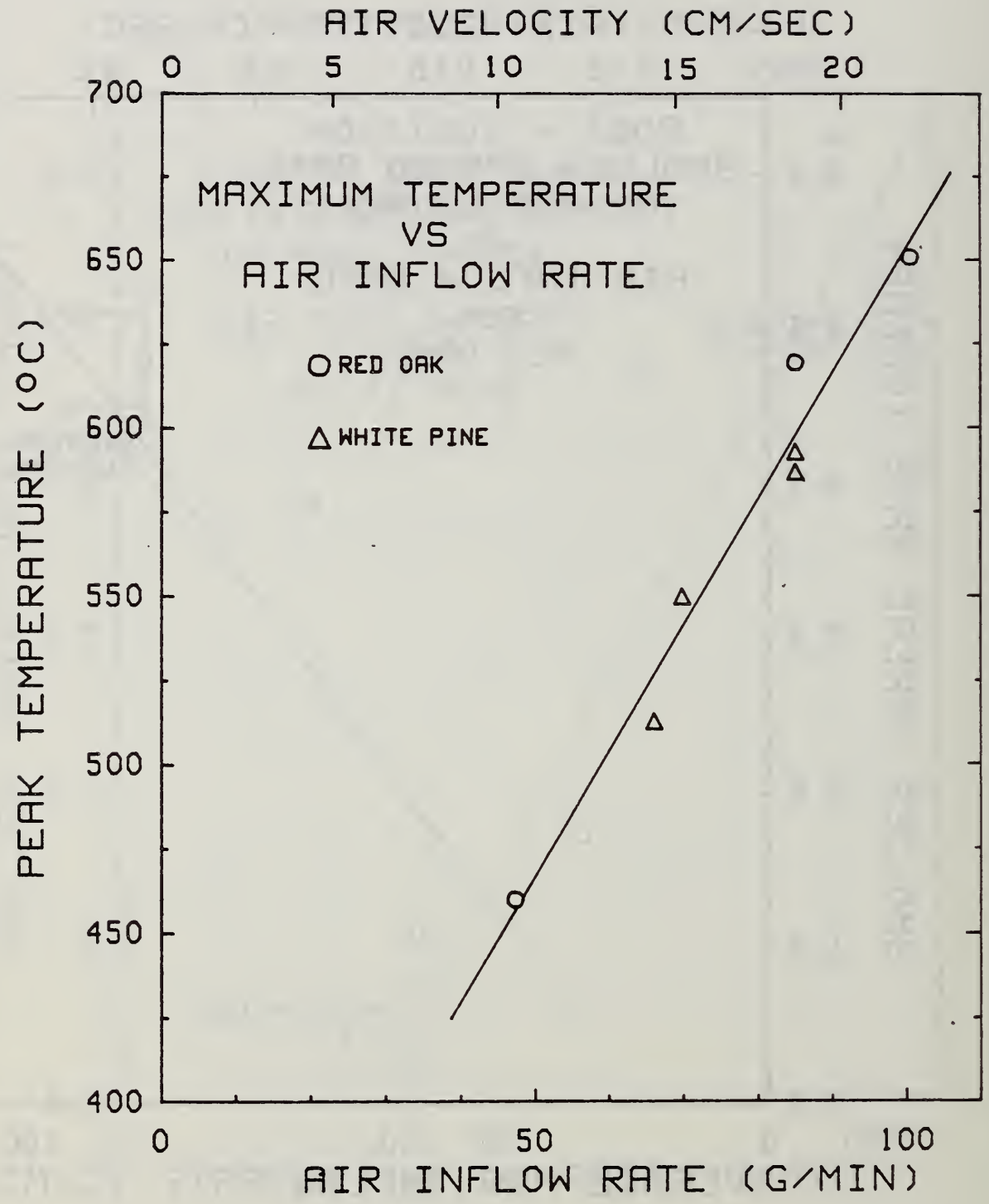

Figure 6. Maximum temperature on the interior surface of the U-channel as a function of air flow for red oak and white pine.

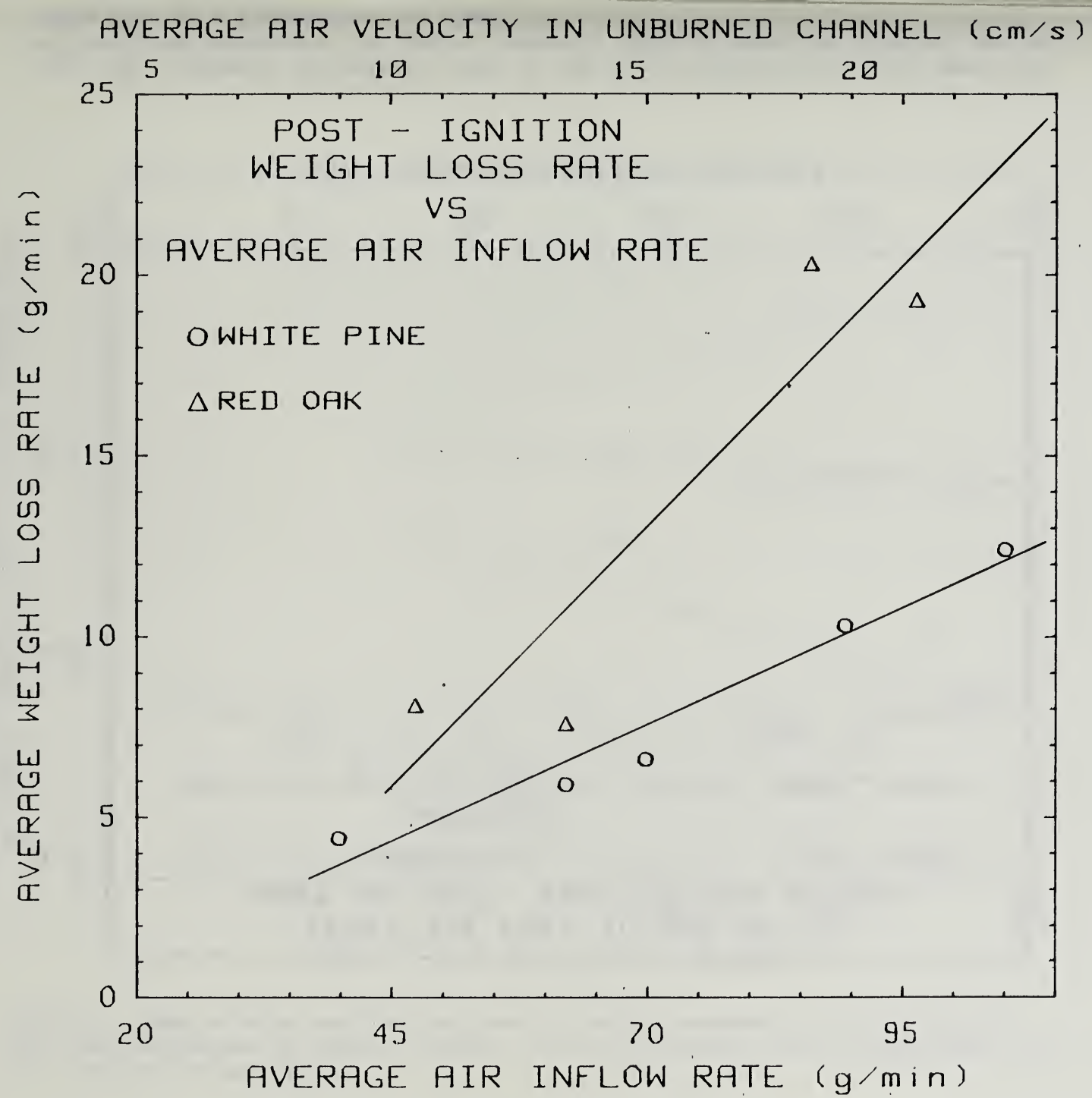

Figure 7. Post-ignition weight loss rate for unction of air flow in the U-channel.

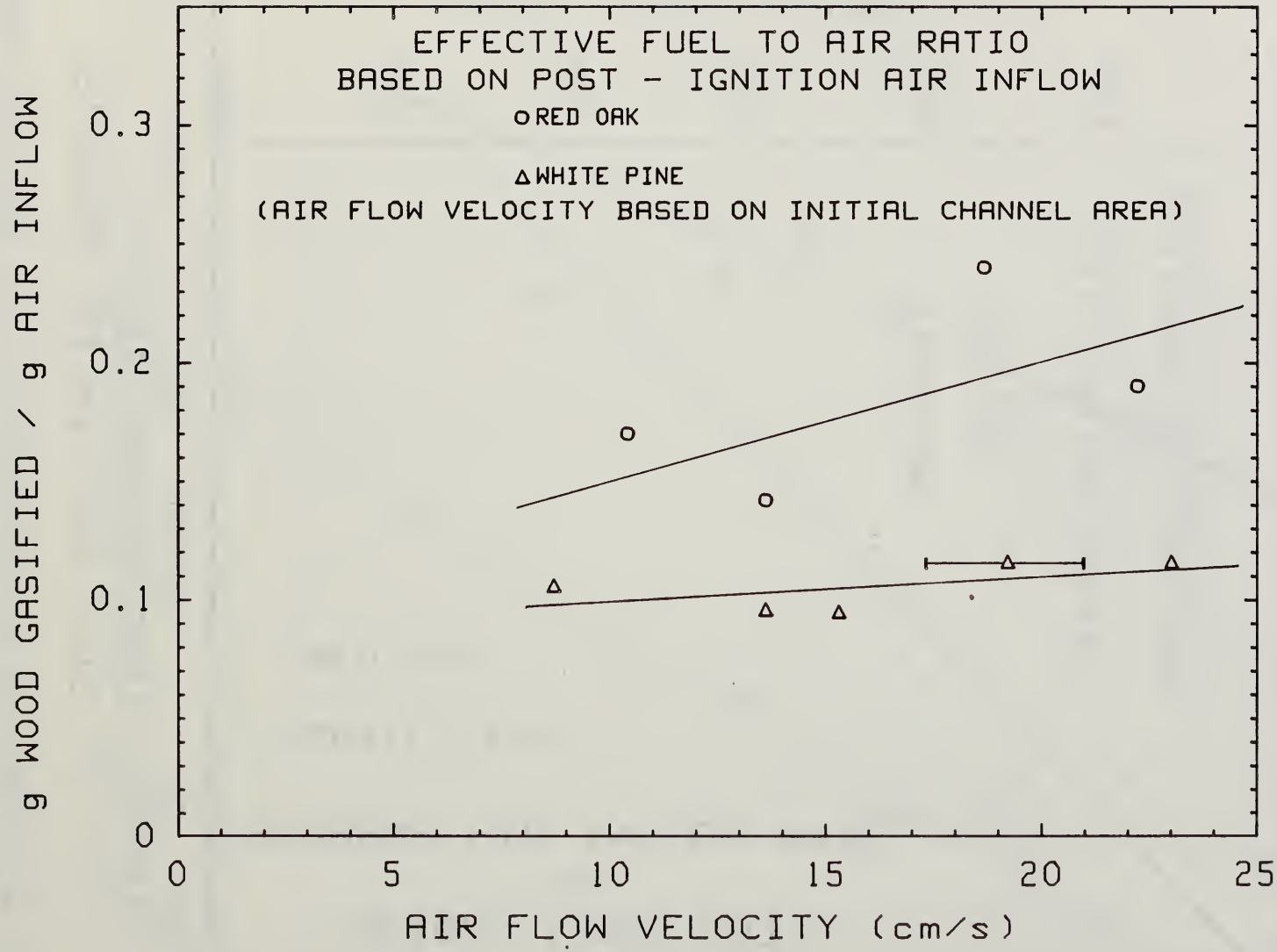

Figure 8. Apparent equivalence ratio of the wood smolder process averaged over all test time subsequent to igniter removal. This is shown for both red oak and white pine as a function of air flow.

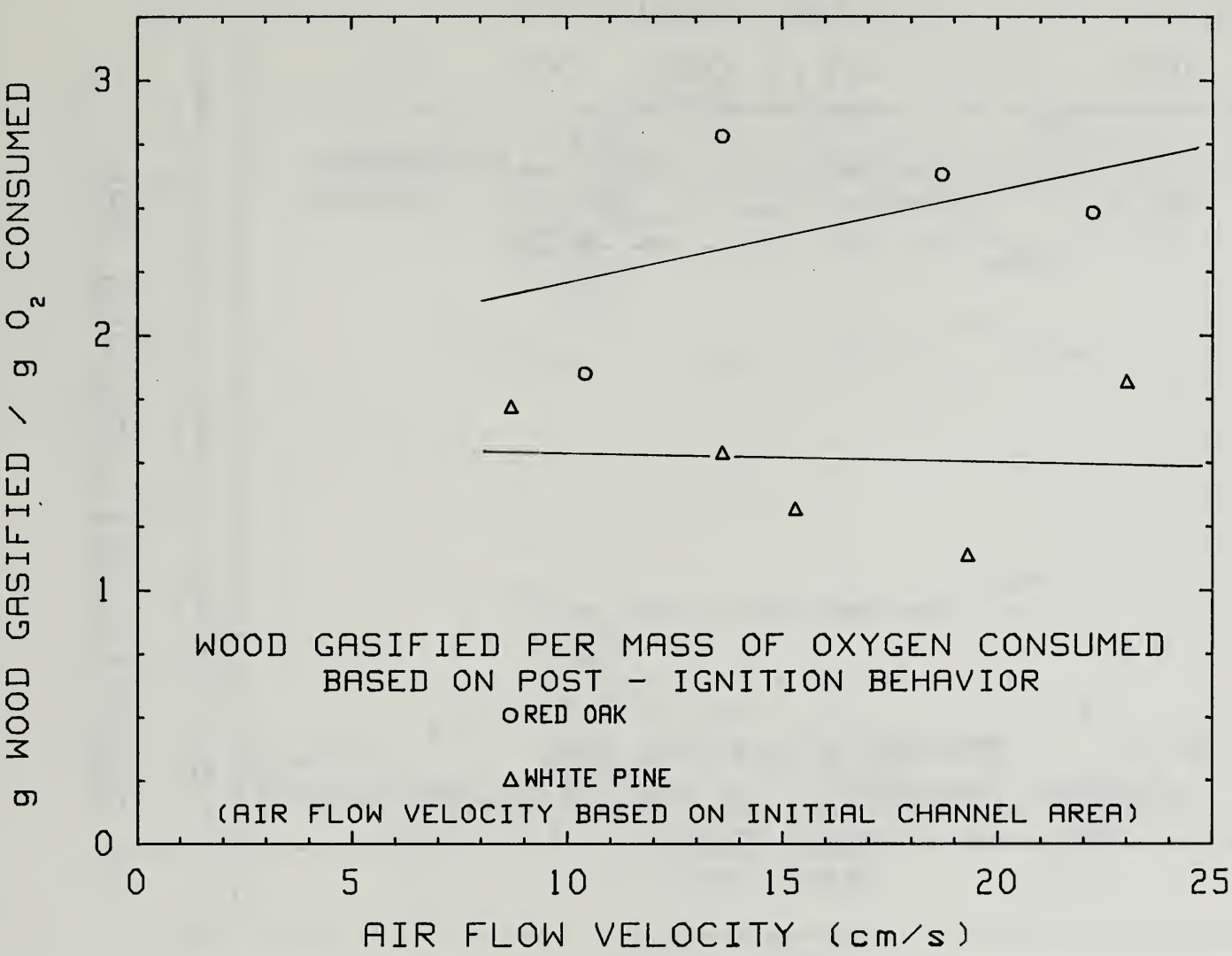

Figure 9. Mass of wood gasified per mass of oxygen consumed averaged over all test time subsequent to igniter removal. This is shown for red oak and white pine as a function of air flow.

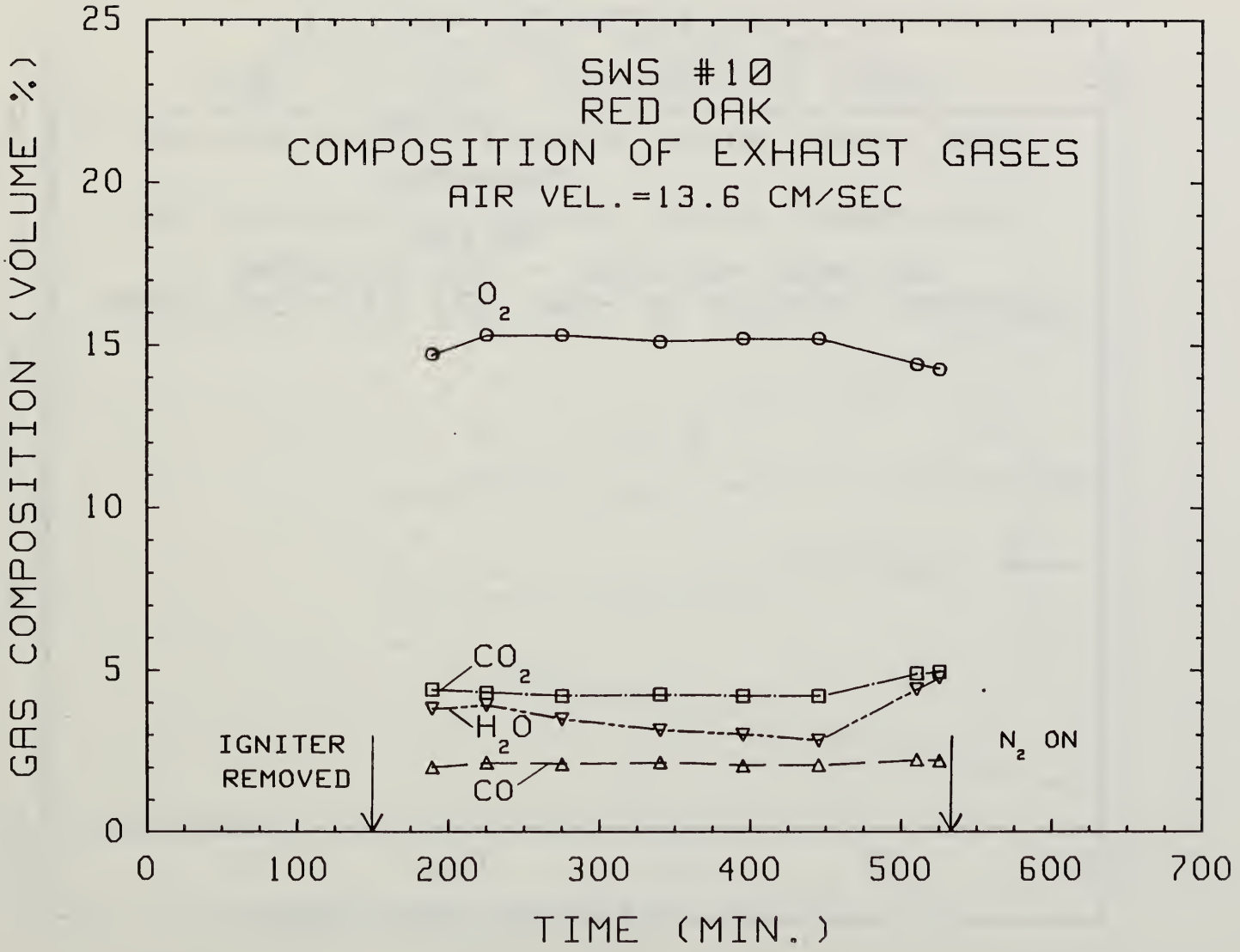

Figure 10. Composition of the exhaust gases from a test of red oak at 13.3 cm/sec air velocity.

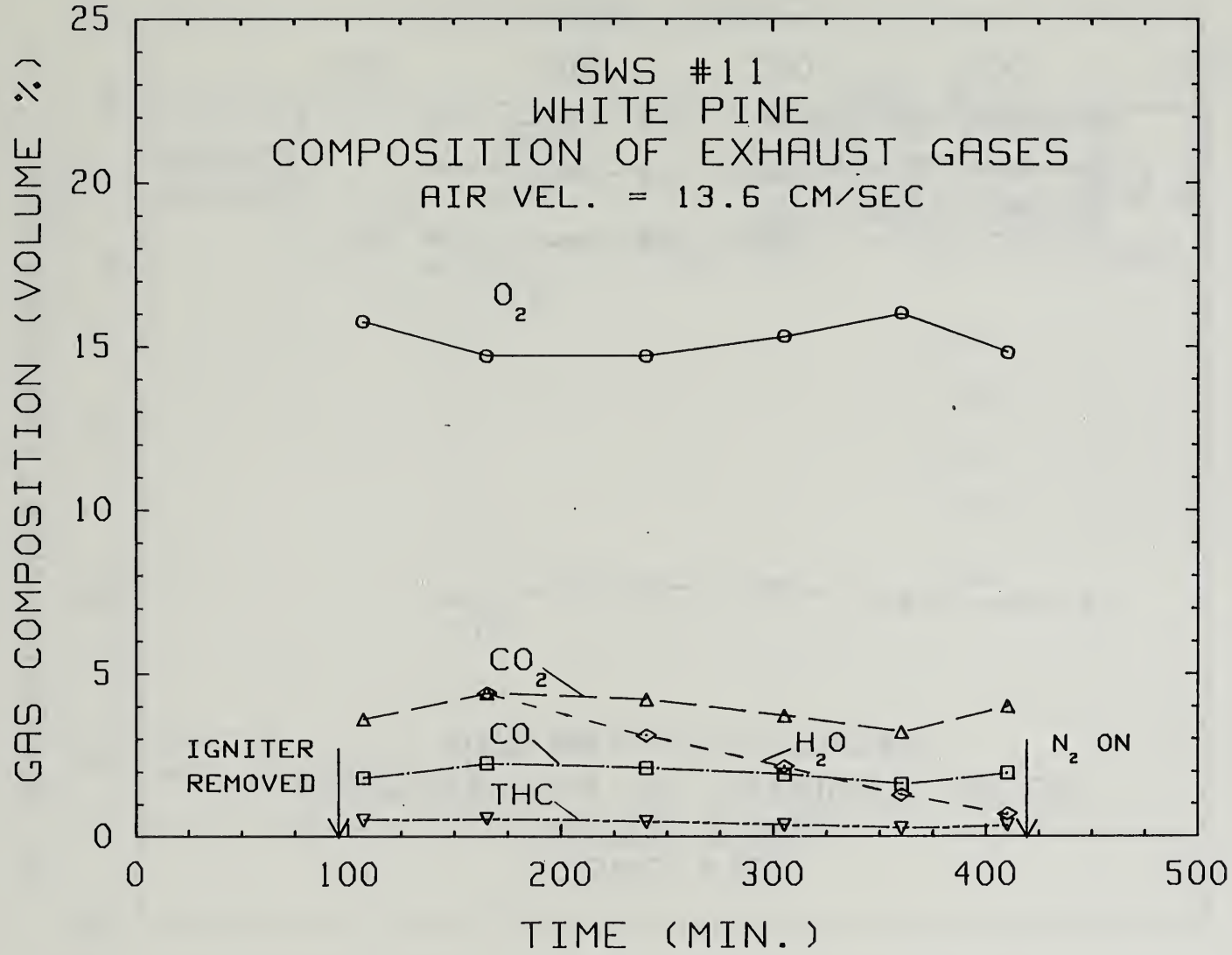

Figure 11. Composition of the exhaust gases from a test of white pine at 13.6 cm/sec air velocity.

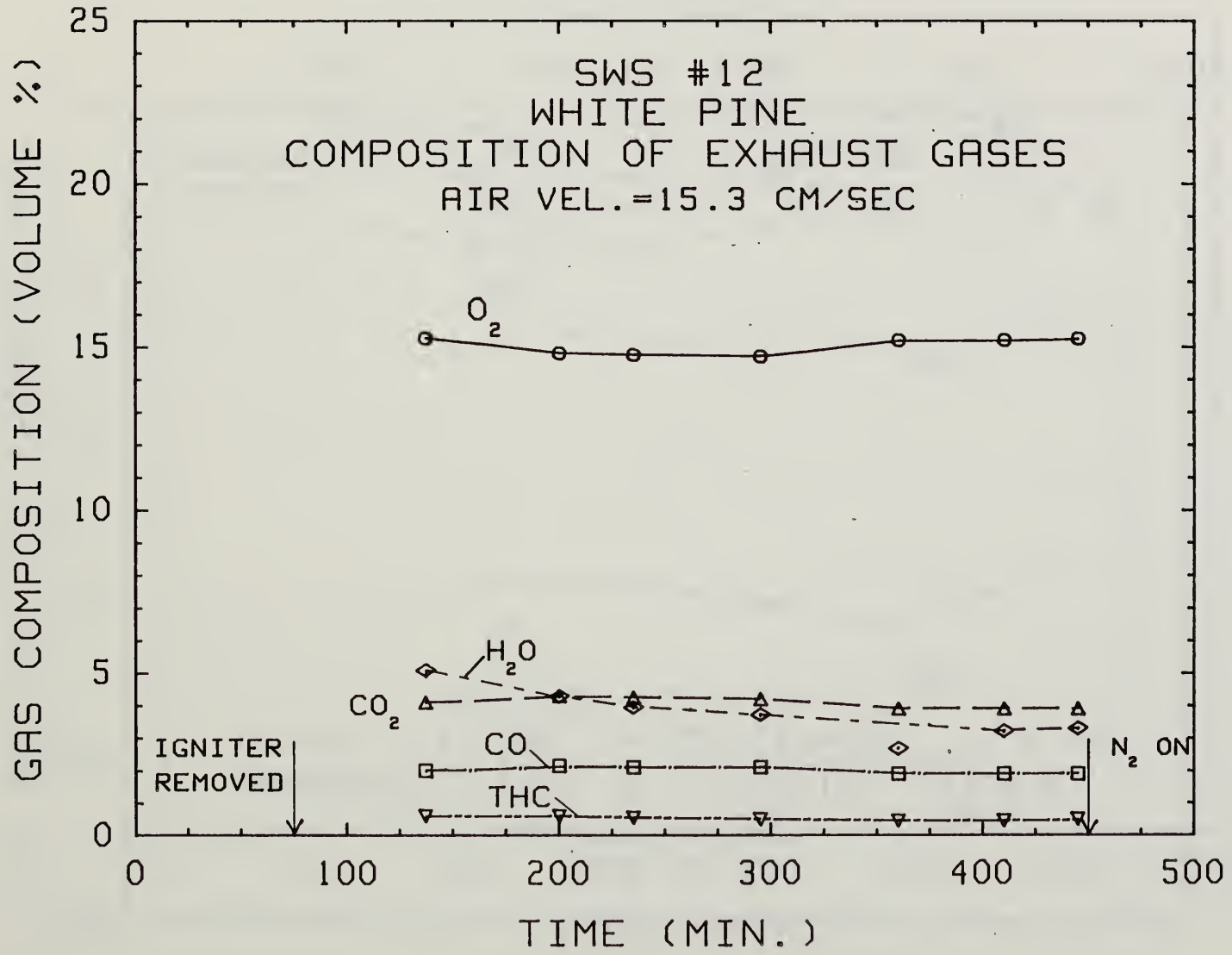

Figure 12. Composition of the exhaust gases from a test of white pine at 15.3 cm/sec air velocity.

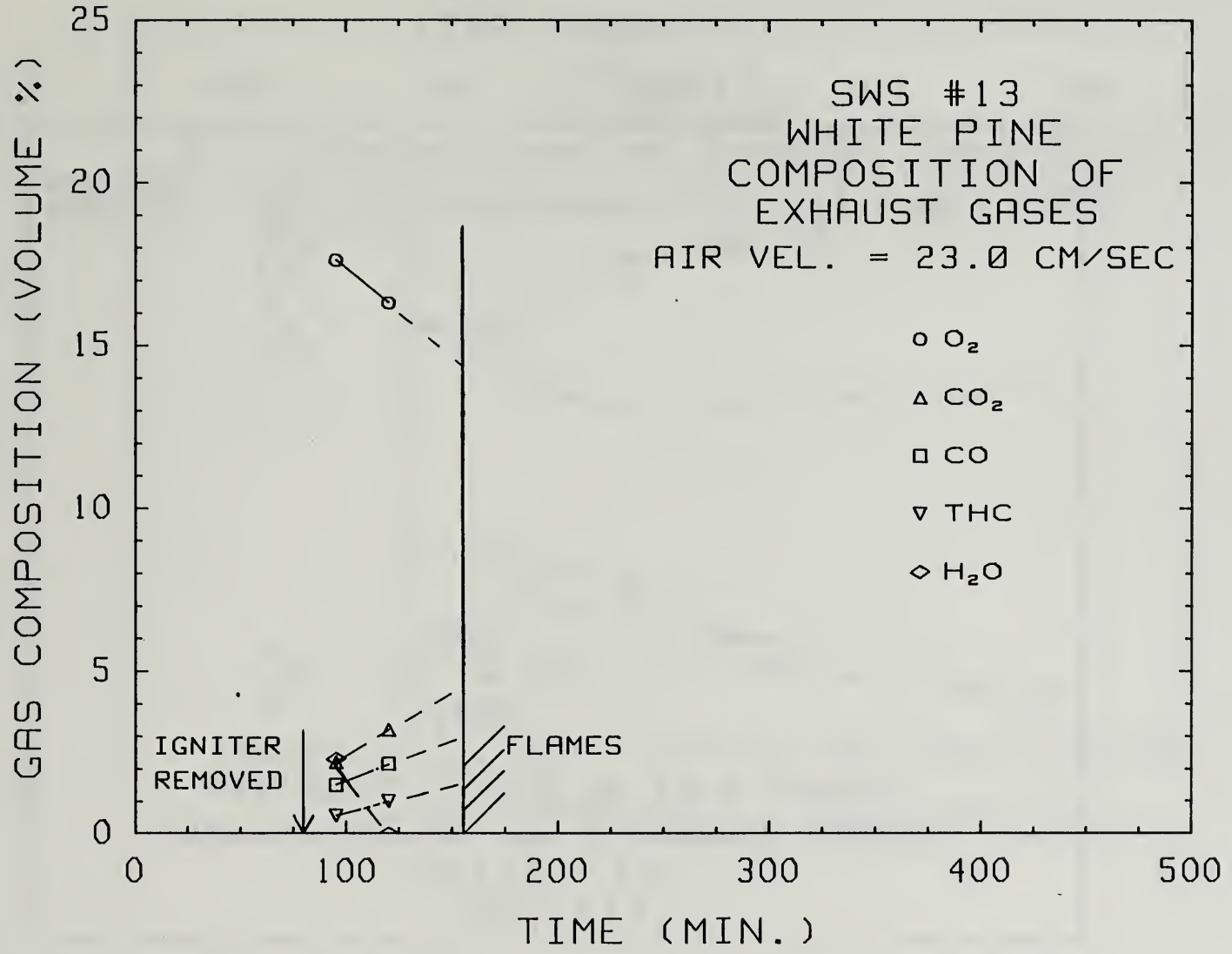

Figure 13. Composition of the exhaust gases from a test of white pine at 23.0 cm/sec air velocity. Flames erupted at the time indicated by the vertical line and the test was terminated.

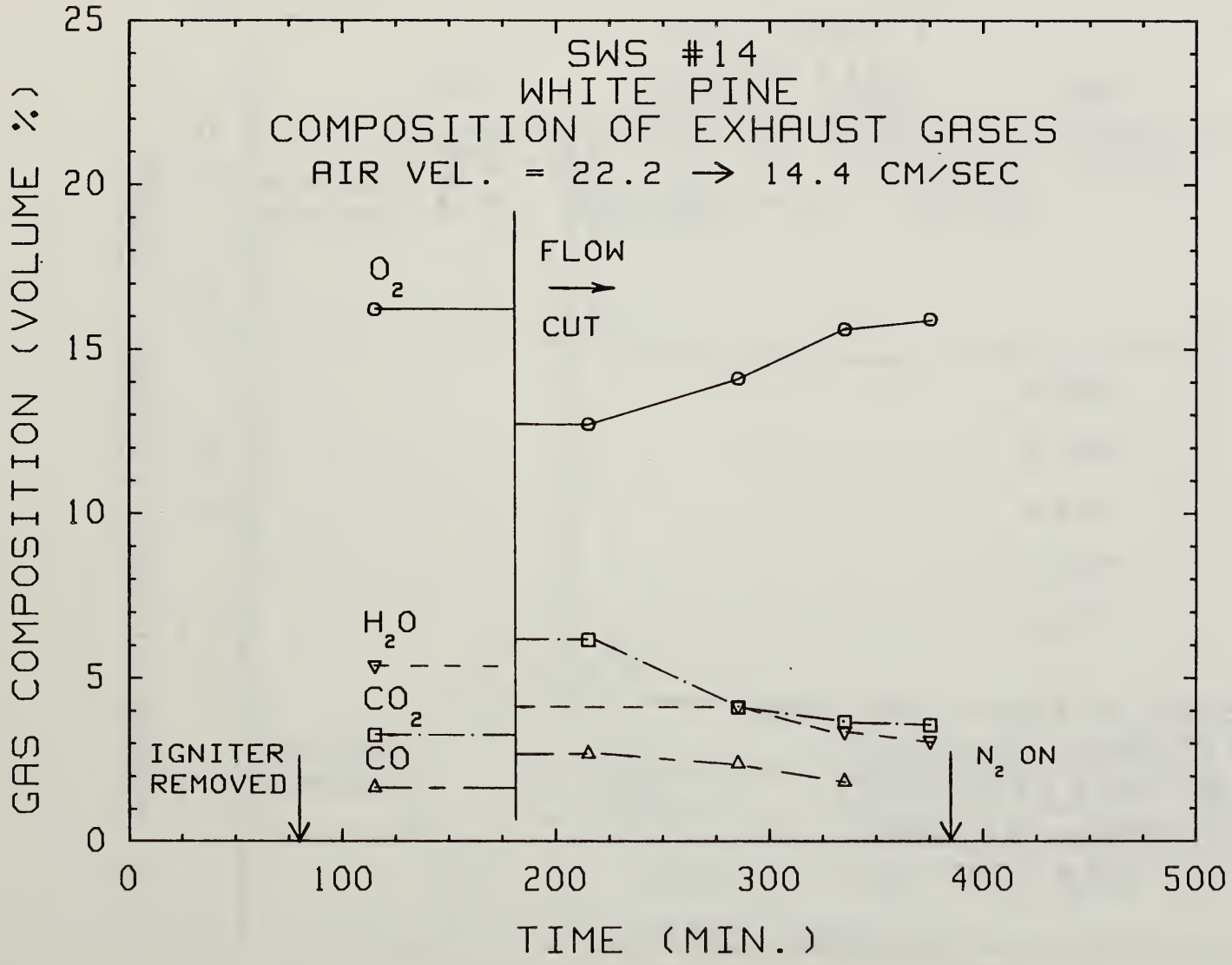

Figure 14. Composition of the exhaust gases from a test of white pine. The air flow velocity was cut abruptly at the time indicated by the vertical line from 22.2 to 14.4 cm/sec. The flow was cut because flaming appeared imminent.

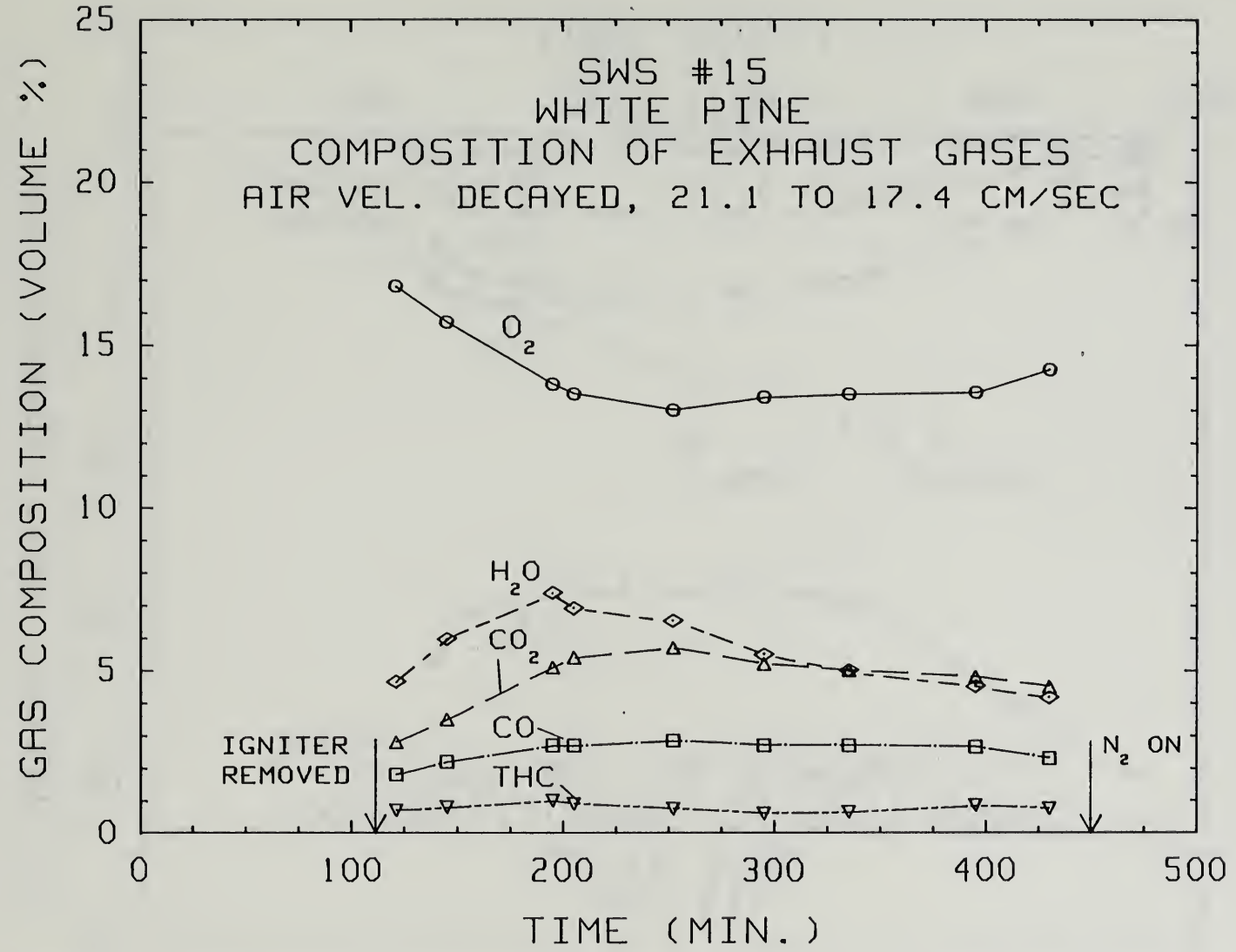

Figure 15. Composition of the exhaust gases from a test of white pine. The air flow decayed slowly through-out the post ignition period from a starting value of 21.2 cm/sec to a final value of 17.4 cm/sec. The decay was caused by narrowing of a point in the exhaust line due to charred deposits.

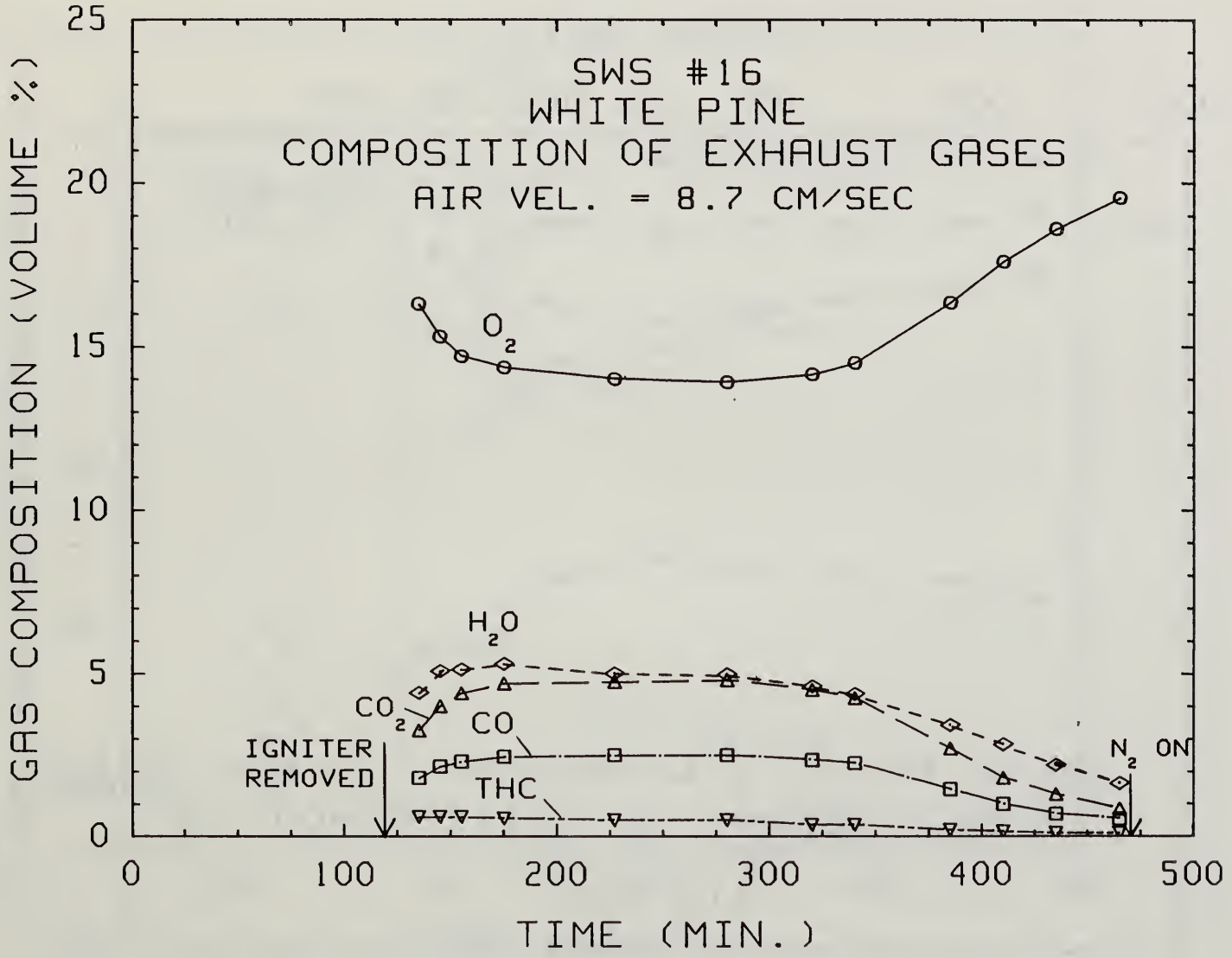

Figure 16. Composition of the exhaust gases from a test of white pine at an air flow velocity of 8.7 cm/sec. The smoldering was virtually extinguished at the time the test was terminated.

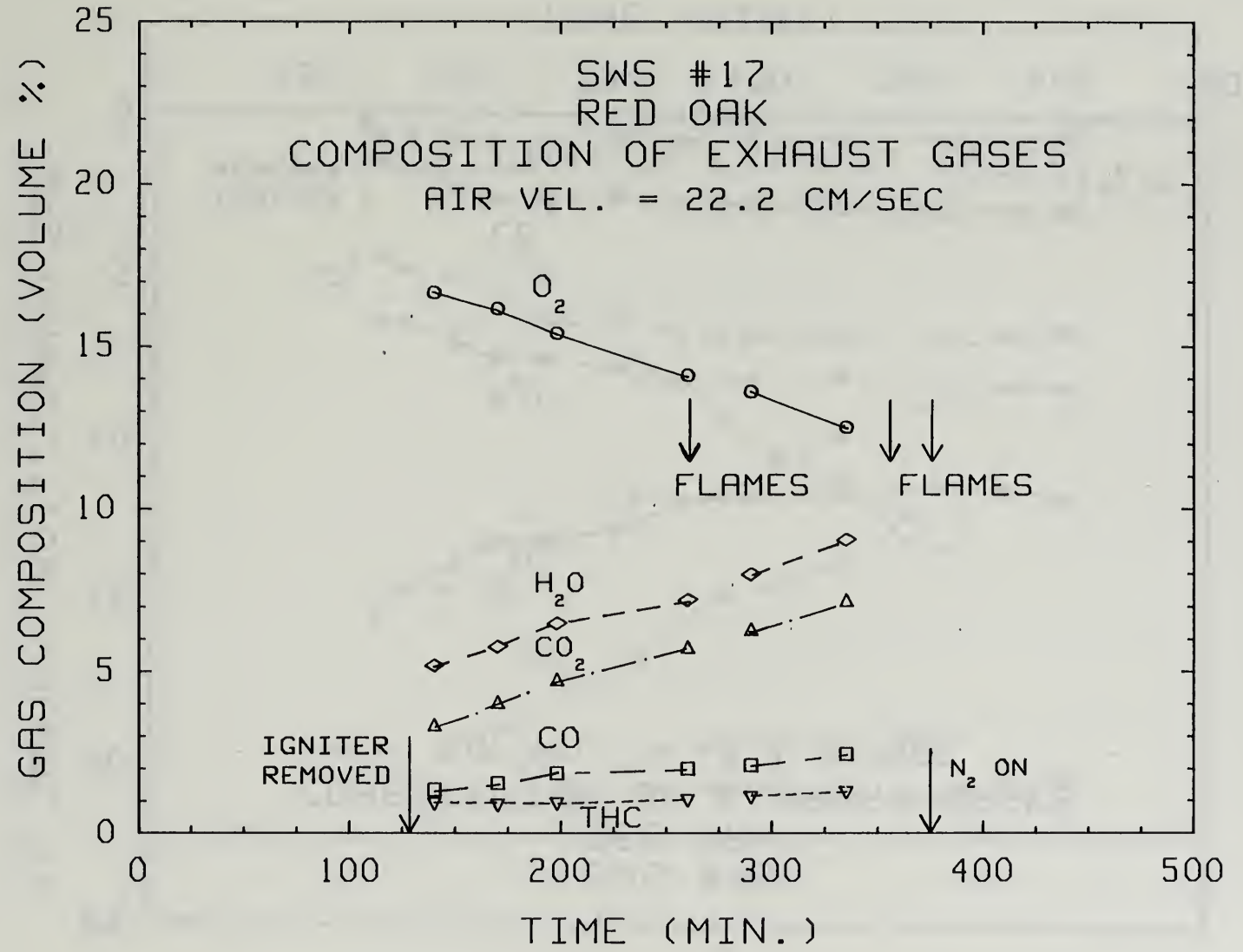

Figure 17. Composition of the exhaust gases from a test of red oak at an air velocity of 22.2 cm/sec. Flames erupted at the three points indicated. The first two flaming episodes were terminated in seconds by cutting the air flow to the chamber; it was resumed within minutes.

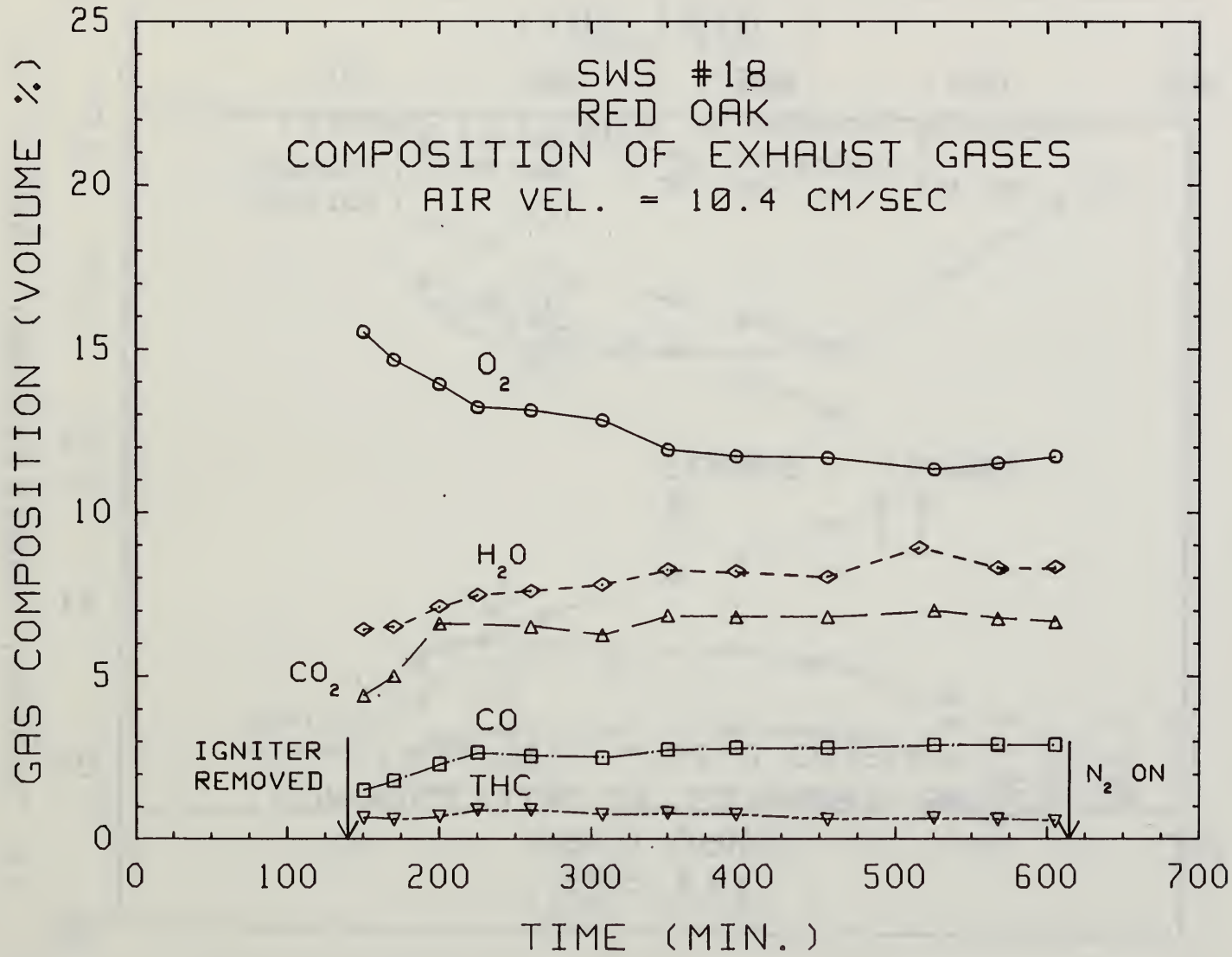

Figure 18. Composition of the exhaust gases from a test of red oak at an air velocity of 10.4 cm/sec.

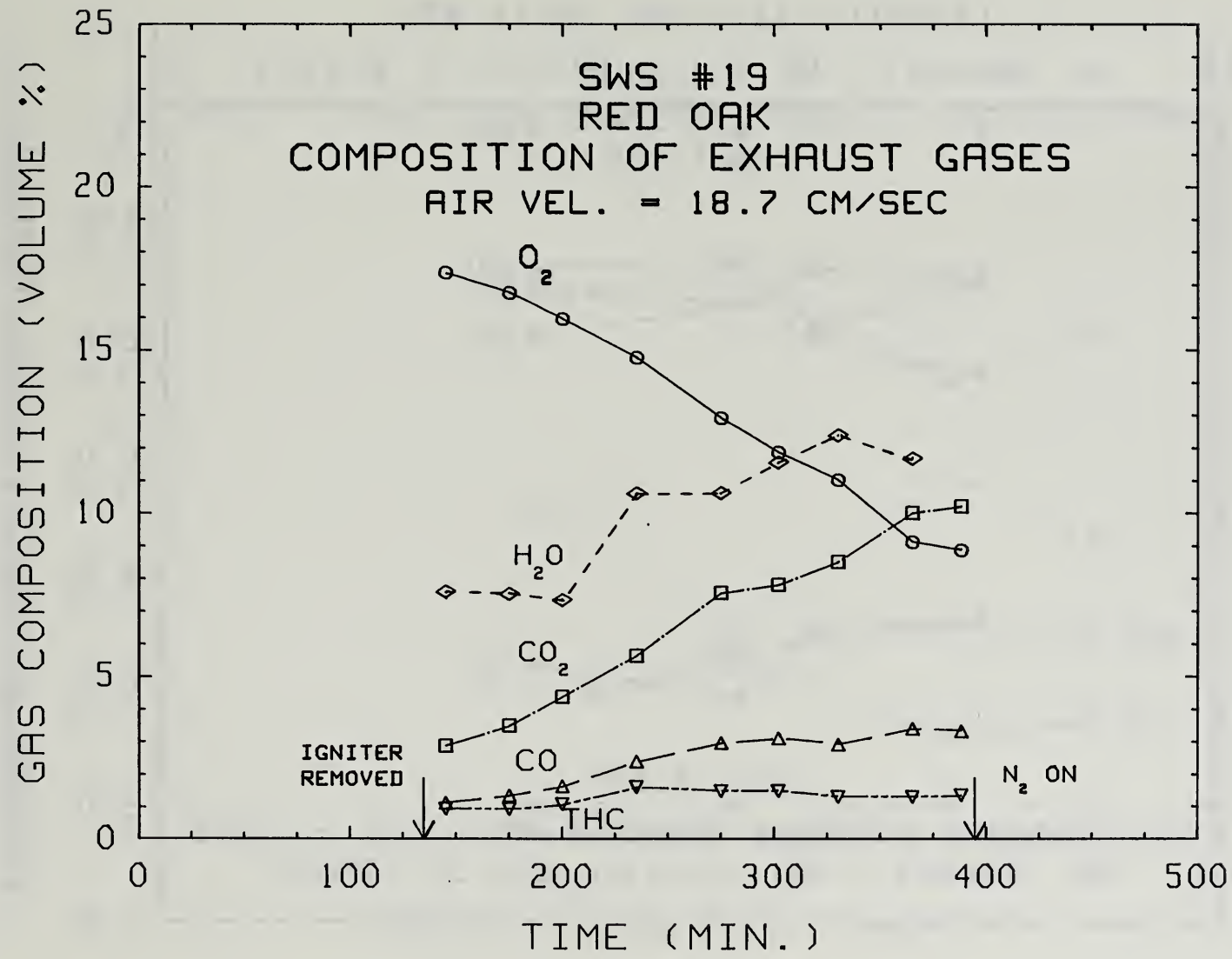

Figure 19. Composition of the exhaust gases from a test of red oak at an air velocity of 18.7 cm/sec. The test was terminated when flames erupted.

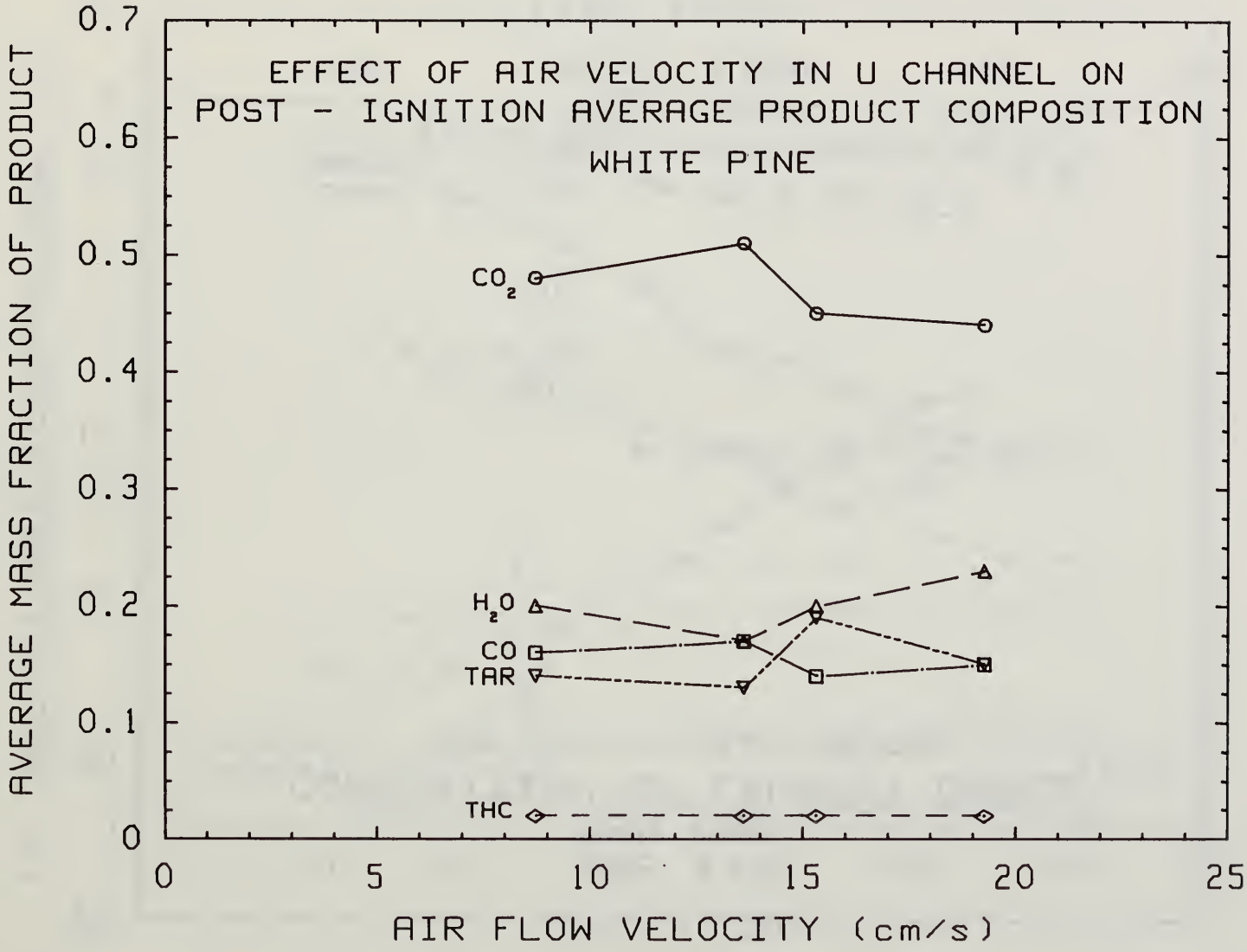

Figure 20. Average composition of products from the surface of the wood for the post-ignition period. Data for white pine as a function of air flow velocity.

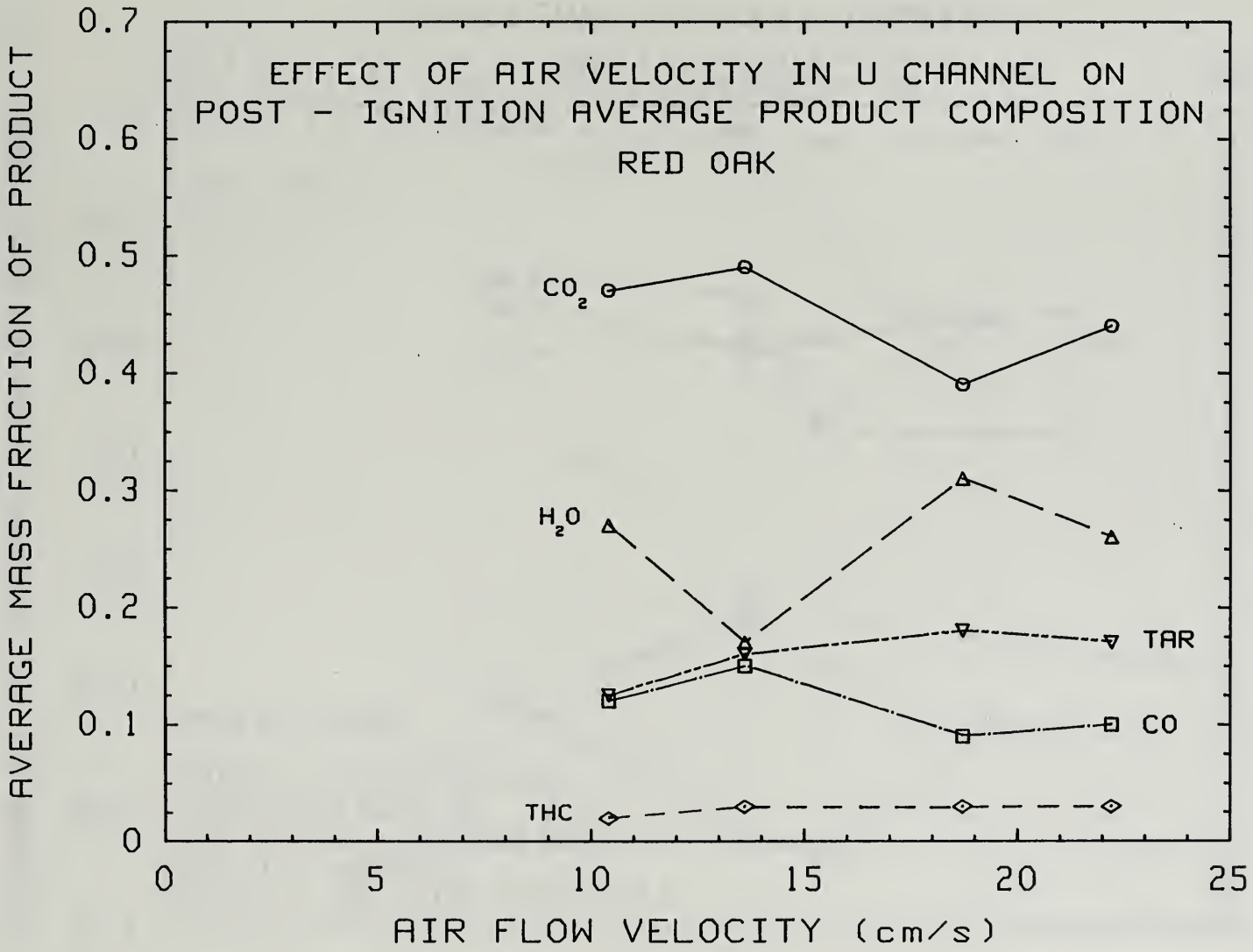

Figure 21. Average composition of products from the surface of the wood for the post-ignition period. Data for red oak as a function of air flow velocity.

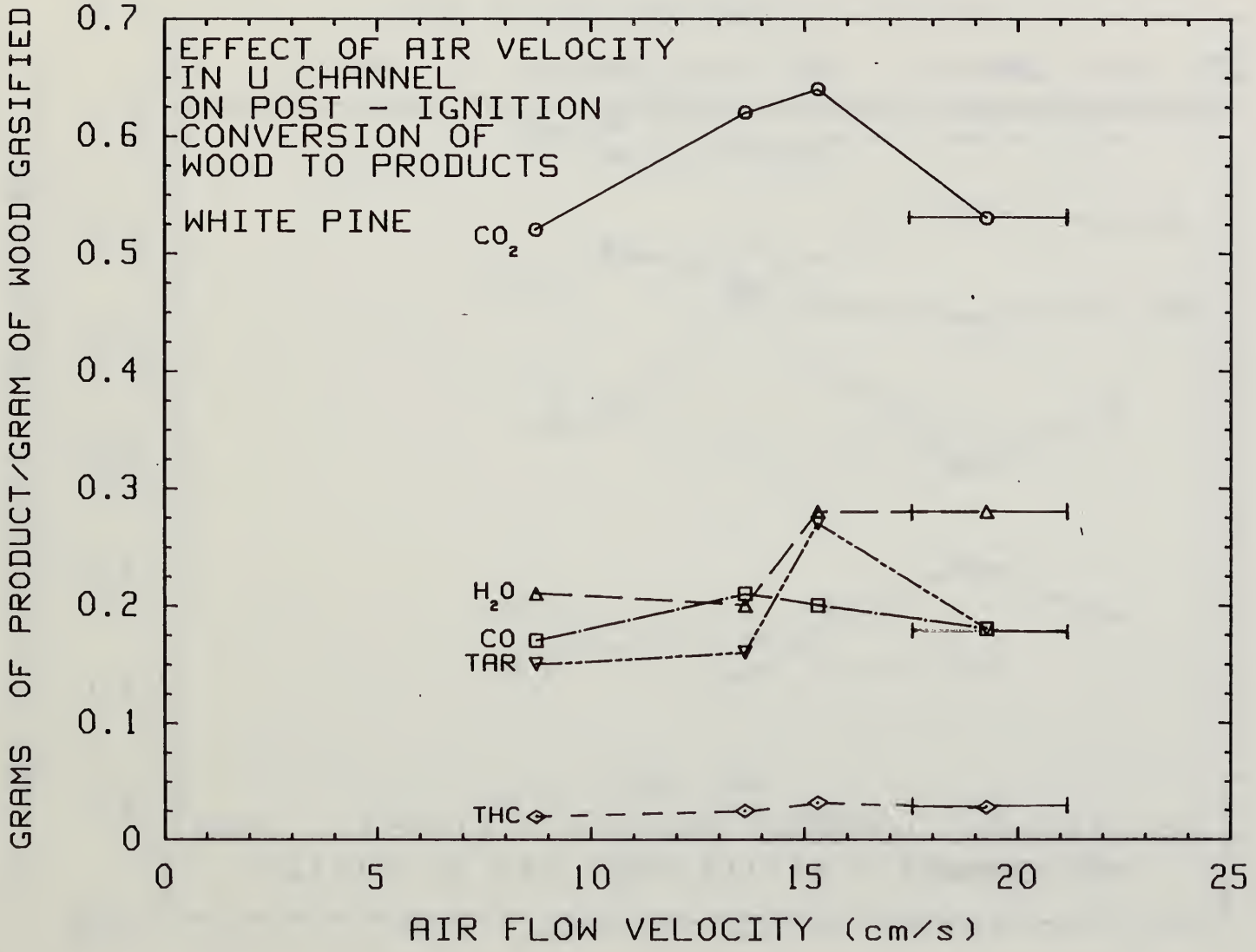

Figure 22. Average yield of products from unit mass of gasified wood for post-ignition period. Data for white pine as a function of air flow velocity.

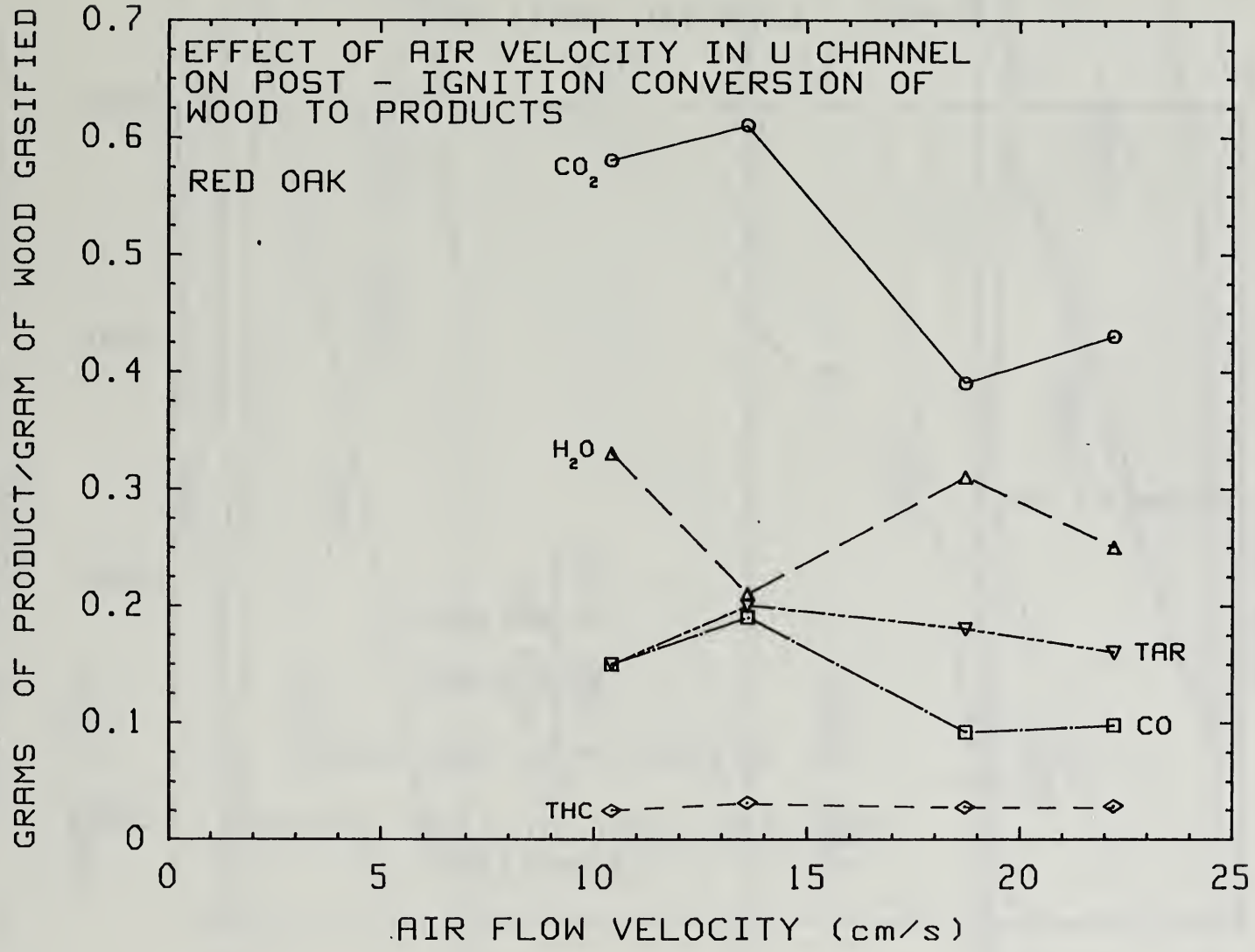

Figure 23. Average yield of products from unit mass of gasified wood for the post-ignition period. Data for red oak as a function of air flow velocity.

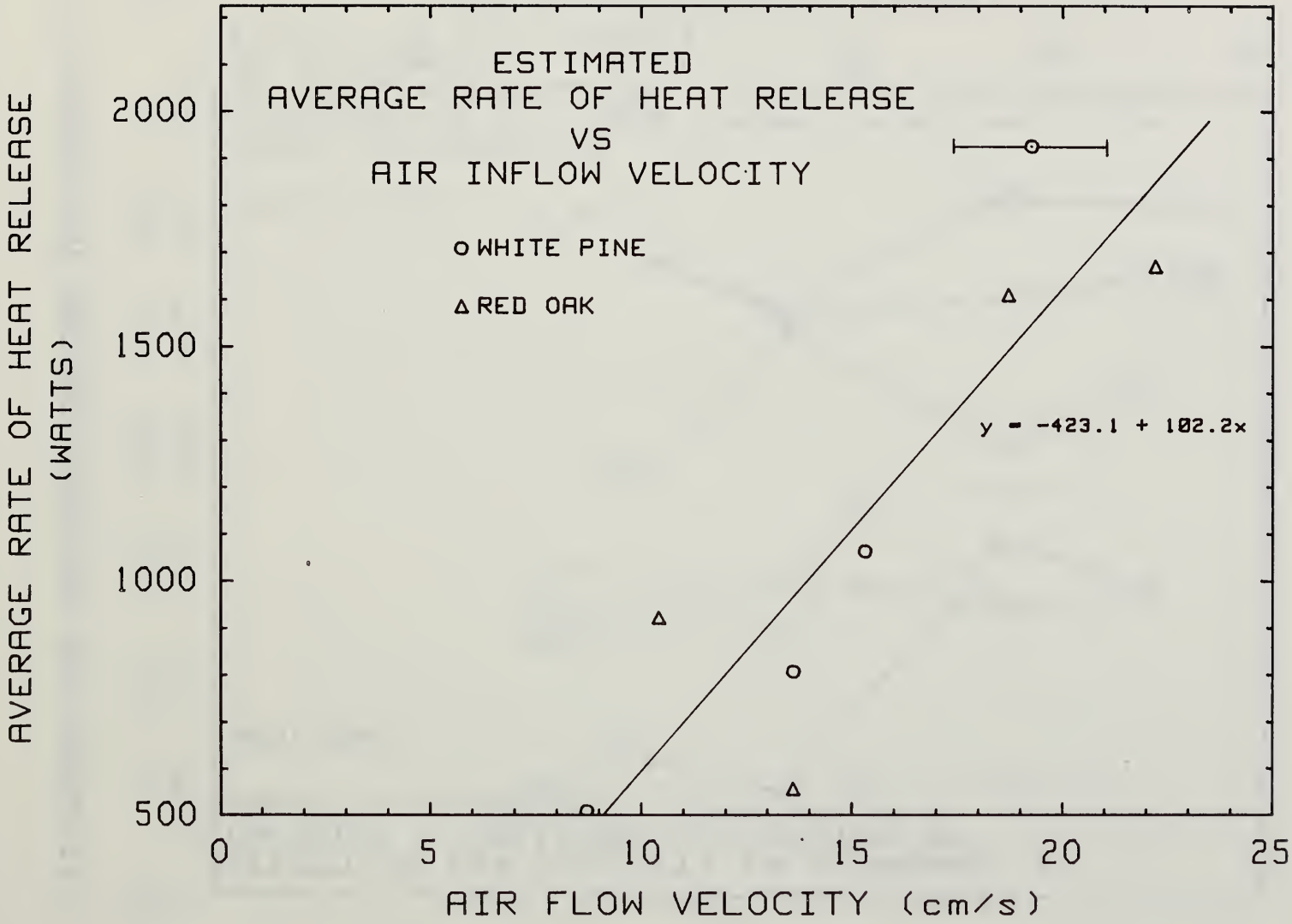

Figure 24. Estimated, post-ignition period, average rate of heat release as a function of air flow velocity. Data for red oak and white pine.

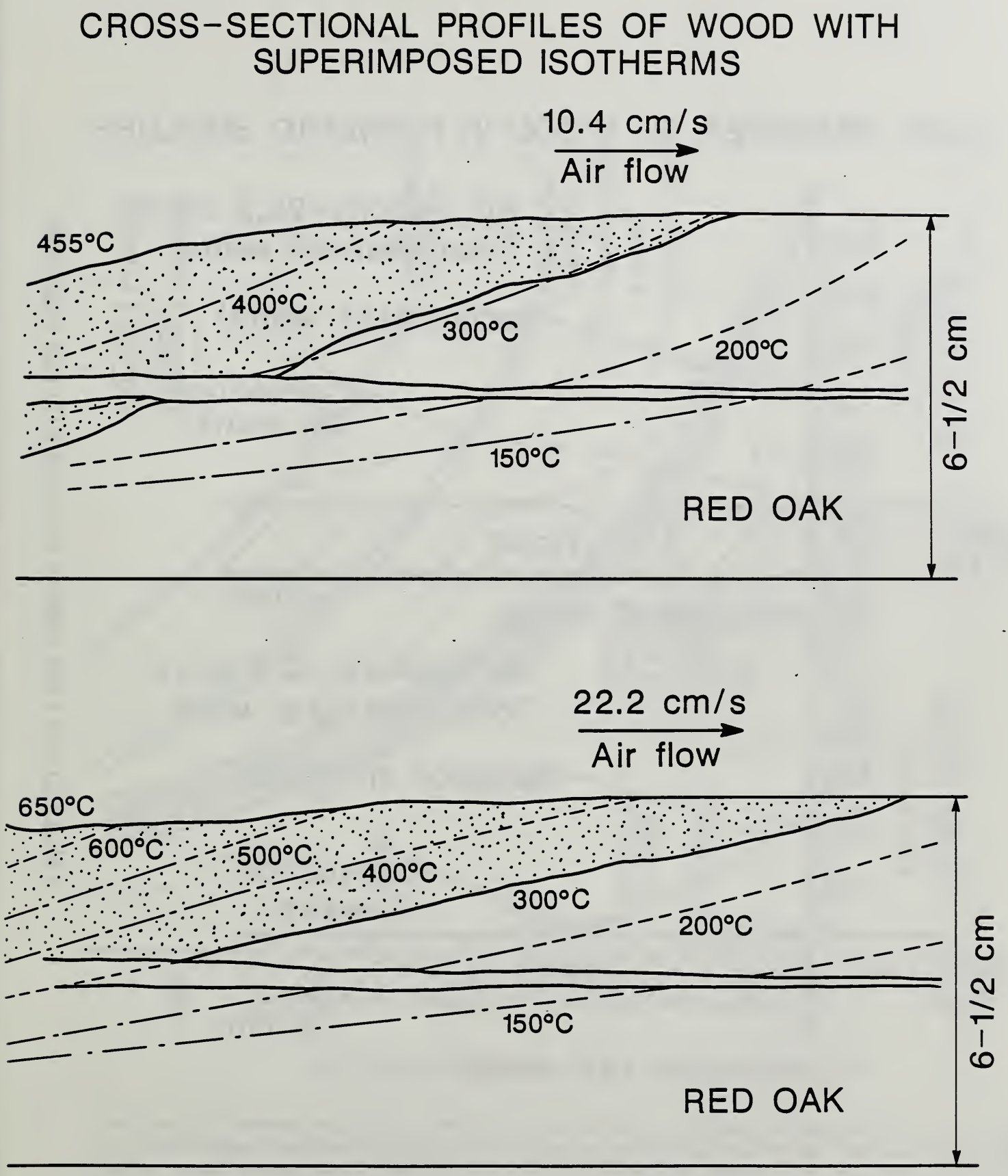

Figure 25. Cross-sectional profiles of red oak at two air flow velocities with superimposed isotherms. Point at which maximum temperature was first reached is also indicated. Note also the gaps at mid-depth due to shrinkage of the two pieces of wood making up the bottom of the U-channel.

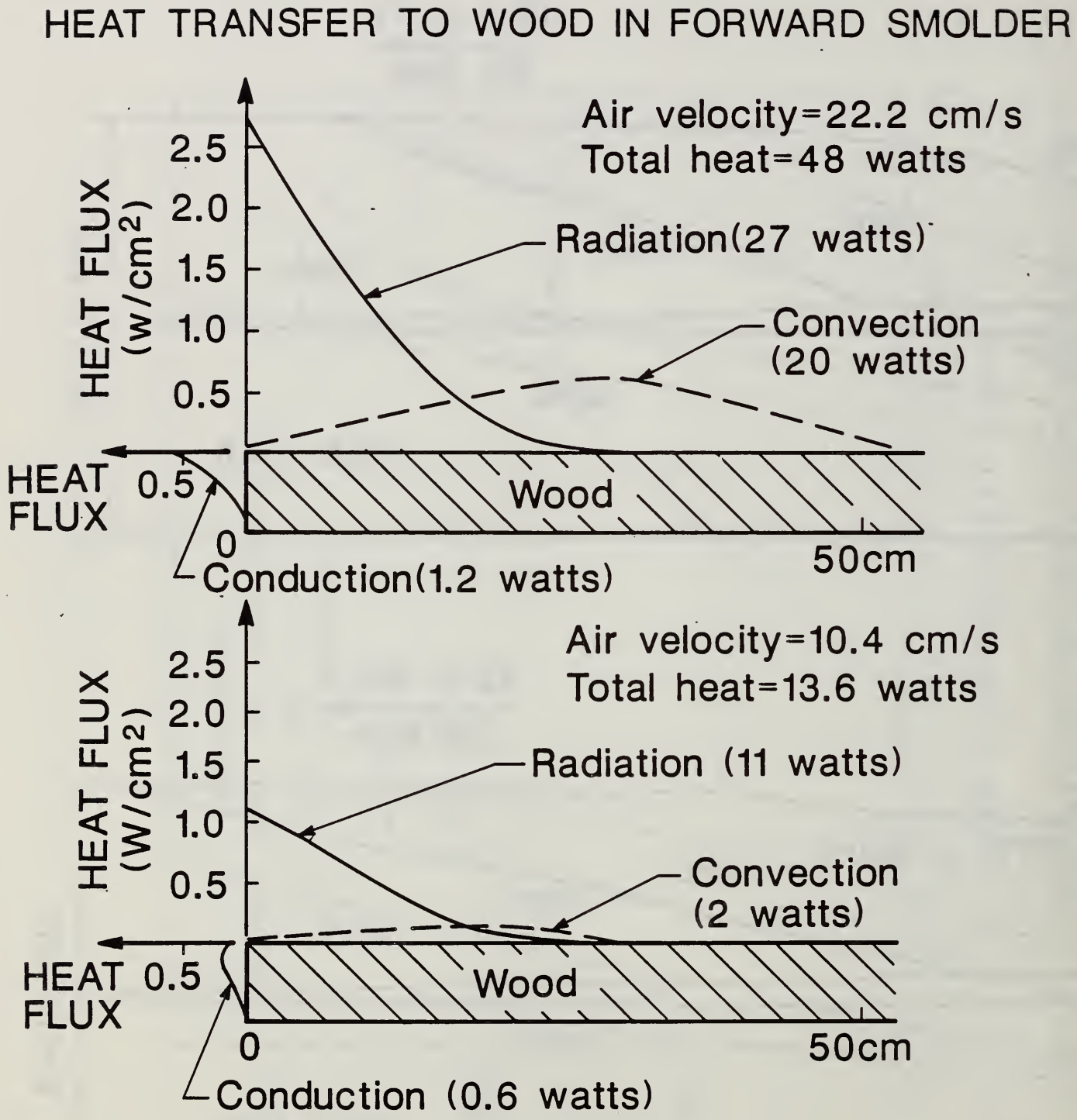

Figure 26. Calculated profiles of three principal heat transfer modes for raising temperature of wood ahead of the point at which the maximum surface temperature is achieved. Profiles are shown for two air flow velocities, superimposed on a cross-section of the base of the U-channel. The quantities in parentheses are the integrals under the curves and they pertain to a one centimeter width of the channel periphery.

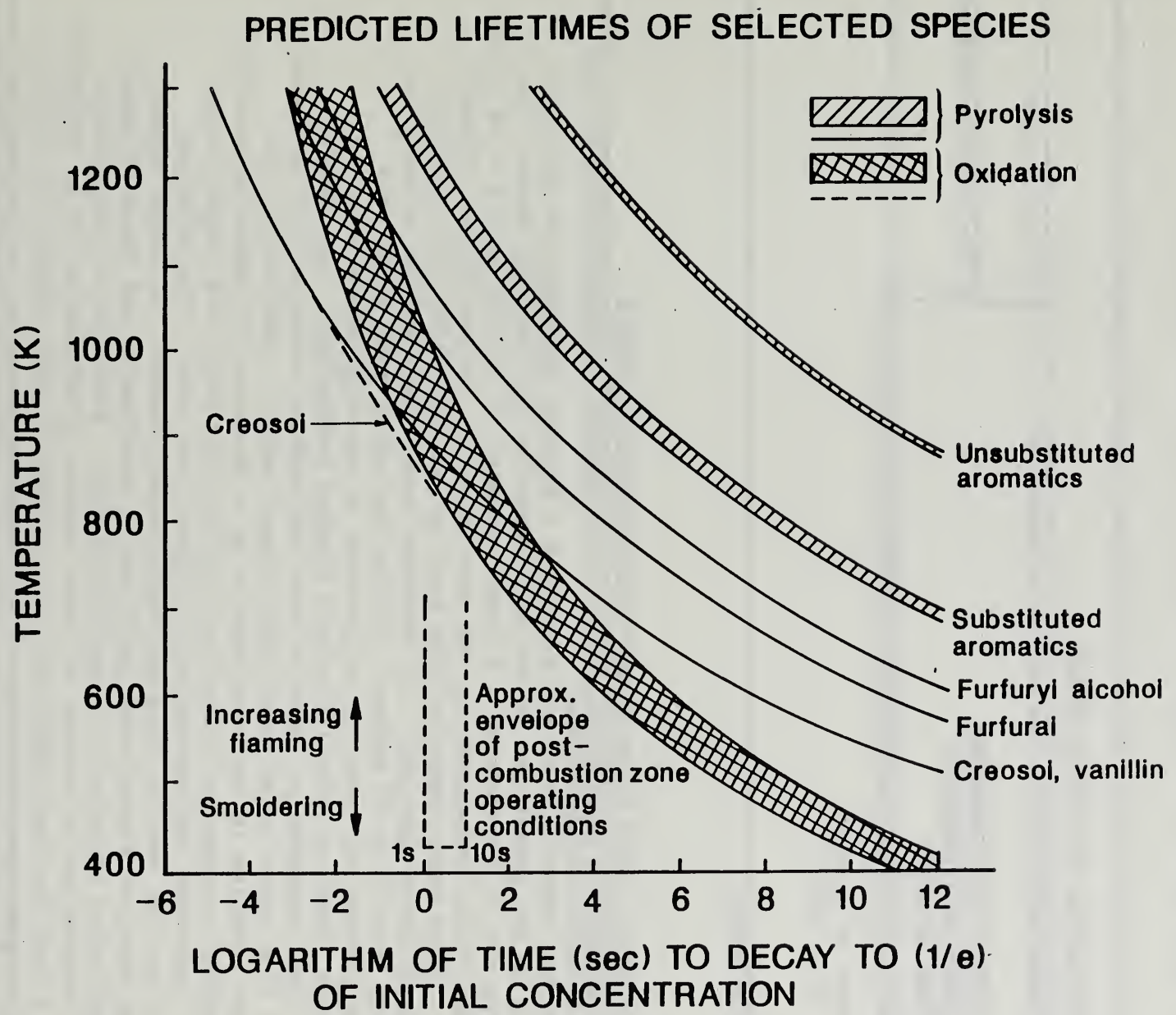

Figure 27. Predicted (1/e) lifetimes of selected species in wood tar as a function of temperature. Predictions are for pyrolytic and oxidative degradation.

NBS-114A (REV. 2-8C)

U.S. DEPT. OF COMM. BIBLIOGRAPHIC DATA SHEET (See instructions)	1. PUBLICATION OR REPORT NO. NBSIR-88/3767	2. Performing Organ. Report No.	3. Publication Date May 1988

4. TITLE AND SUBTITLE

Products of Wood Smolder and Their Relation to Wood-Burning Stoves

5. AUTHOR(S)

Thomas J. Ohlemiller and Walter Shaub

6. PERFORMING ORGANIZATION (If joint or other than NBS, see instructions)

NATIONAL BUREAU OF STANDARDS
U.S. DEPARTMENT OF COMMERCE
GAITHERSBURG, MD 20899

7. Contract/Grant No.

8. Type of Report & Period Covered

9. SPONSORING ORGANIZATION NAME AND COMPLETE ADDRESS (Street, City, State, ZIP)

U.S. Department of Energy
Washington, D.C. 20585

10. SUPPLEMENTARY NOTES

☐ Document describes a computer program; SF-185, FIPS Software Summary, is attached.

11. ABSTRACT (A 200-word or less factual summary of most significant information. If document includes a significant bibliography or literature survey, mention it here)

The smoldering combustion of solid wood is a process pertinent to both fire safety and to the generation of air pollutants in wood burning stoves. The wood sample was in the form of a U-shaped channel 74 cm long with 6.4 cm thick walls. Smoldering propagated in the same direction as the airflow (forward smolder). Tests were conducted with both red oak and white pine and both woods behaved quite similarly. In separate tests the air flow velocity was varied from about 9 to 22 cm/sec. At the low end of this range, the smoldering process was prone to extinction; at the high end it was increasingly likely to transition into flaming combustion. The smolder velocity, peak temperature, rate of heat and product evolution all increased over this flow range in an essentially linear manner. Analysis of the temperature profiles in the wood pointed to a dominance of radiative transfer in the smolder propagation process at low air flow rates and roughly equal roles for radiation and convection at higher flow rates. The principal species in the tar evolved from smoldering wood resemble, in large degree, those from previous forced wood gasification experiments and those obtained from a wood stove operated in a smoldering mode. Estimates of the kinetic rates of destruction of several of these species by pyrolysis and by oxidation point to a need for some additional heat source if these species are to be destroyed by gas phase processes.

12. KEY WORDS (Six to twelve entries; alphabetical order; capitalize only proper names; and separate key words by semicolons)

air pollution; combustion products; smoke; smoldering combustion; wood; wood stoves

13. AVAILABILITY

☒ Unlimited

☐ For Official Distribution. Do Not Release to NTIS

☐ Order From Superintendent of Documents, U.S. Government Printing Office, Washington, D.C. 20402.

☒ Order From National Technical Information Service (NTIS), Springfield, VA. 22161

14. NO. OF PRINTED PAGES 91

15. Price 13.95